The Influence of Chemical and Mineral Compositions on the Parameterization of Immersion Freezing by Volcanic Ash Particles

N. S. Umo[1] , R. Ullrich[1] , E. C. Maters[2,3] , I. Steinke[1,4] , N. Benker[5] , K. Höhler[1] , R. Wagner[1] , P. G. Weidler[6] , G. A. Hoshyaripour[7] , A. Kiselev[1] , U. Kueppers[8] , K. Kandler[5] , D. B. Dingwell[8], T. Leisner[1] , and O. Möhler[1]

[1]Institute of Meteorology and Climate Research - Atmospheric Aerosol Research, Karlsruhe Institute of Technology, Eggenstein-Leopoldshafen, Germany, [2]School of Earth and Environment, Institute for Climate and Atmospheric Science, University of Leeds, Leeds, UK, [3]Department of Chemistry, University of Cambridge, Cambridge, UK, [4]Atmospheric Sciences and Global Change Division, Pacific Northwest National Laboratory, WA, Richland, USA, [5]Institute of Applied Geosciences, Technical University Darmstadt, Darmstadt, Germany, [6]Institute of Functional Interfaces, Karlsruhe Institute of Technology, Eggenstein-Leopoldshafen, Germany, [7]Department of Tropospheric Research, Institute of Meteorology and Climate Research, Karlsruhe Institute of Technology, Eggenstein-Leopoldshafen, Germany, [8]Department of Earth and Environmental Sciences, Ludwig-Maximilians-Universität (LMU), Munich, Germany

Abstract Volcanic ash (VA) from explosive eruptions contributes to aerosol loadings in the atmosphere. Aside from the negative impact of VA on air quality and aviation, these particles can alter the optical and microphysical properties of clouds by triggering ice formation, thereby influencing precipitation and climate. Depending on the volcano and eruption style, VA displays a wide range of different physical, chemical, and mineralogical properties. Here, we present a unique data set on the ice nucleation activity of 15 VA samples obtained from different volcanoes worldwide. The ice nucleation activities of these samples were studied in the Aerosol Interaction and Dynamics in the Atmosphere (AIDA) cloud simulation chamber as well as with the Ice Nucleation Spectrometer of the Karlsruhe Institute of Technology (INSEKT). All VA particles nucleated ice in the immersion freezing mode from 263 to 238K with ice nucleation active site (INAS) densities ranging from $\sim 10^5$ to 10^{11} m^{-2}, respectively. The variabilities observed among the VA samples, at any given temperature, range over 3.5 orders of magnitude. The ice-nucleating abilities of VA samples correlate to varying degrees with their bulk pyroxene and plagioclase contents as a function of temperature. We combined our new data set with existing literature data to develop an improved ice nucleation parameterization for natural VA in the immersion freezing mode. This should be useful for modeling the impact of VA on clouds.

Plain Language Summary Volcanic ash particles, which are generated during volcanic eruptions, can initiate ice formation in clouds. The clouds formed by these volcanic ash particles can influence precipitation, and in turn, weather and climate. In our study, we investigated the ability with which volcanic ash particles form ice in clouds. We performed our study in a state-of-the-art aerosol and cloud simulation chamber and on a cold-stage instrument. The findings show that volcanic ash particles can form ice as effectively as mineral dust particles or their components. These results will help scientists to have a better understanding of the impact of volcanic ash particles on clouds.

1. Introduction

Explosive volcanic eruptions are accompanied by the emission of a large amount of ash particles (e.g., 384 Tg at Eyjafjallajökull in 2010 [Gudmundsson et al., 2012]). These airborne particles can impact air quality and climate and thereby indirectly affect human health, the aviation industry, precipitation, and the built environment (Casadevall, 1994; Dingwell et al., 2012; Hansen et al., 1992; Robock, 2000; Wilson et al., 2012; Yano et al., 2010). As an example, the 2010 Icelandic volcanic eruption of Eyjafjallajökull led to a restriction in air traffic which affected over 8.5 million passengers and associated commerce in Europe (Alexander, 2013). The atmospheric residence time of volcanic ash (VA) particles can range from hours to weeks depending on the particle size, shape, density, the eruption properties, and the current meteorology

(Rose & Durant, 2009). Since the Eyjafjallajökull eruption, there has been an increased research interest in the impacts of VA on the Earth system and across different fields of human endeavor (Hlodversdottir et al., 2016; Ulfarsson & Unger, 2011).

VA particles in the atmosphere may be (a) recently emitted from explosive eruptions or (b) resuspended from older volcanic deposits by strong winds. VA particles are capable of being transported to high altitudes and over long distances. For example, ash particles larger than 20 μm have been detected in the atmosphere after long-range transport from the source region (Ansmann et al., 2010). Hence, they may have far-reaching impacts on the Earth system (Ayris & Delmelle, 2012), including interaction with solar and terrestrial radiation in the atmosphere (Minnis et al., 1993). In the proximity of volcanoes, VA particles disperse in a so-called volcanic cloud along with co-emitted water vapor, sulfuric acid particles, and other magmatic gases (e.g., SO_2, HCl). This mixture can significantly perturb the atmospheric charge (Behnke et al., 2013; Brook et al., 1974; Prata, 2009). Aside from directly modulating solar radiation in the Earth's atmosphere and forming volcanic clouds, VA can also influence cloud formation processes (Durant et al., 2008). This interaction with clouds can occur by the ash particles acting either as cloud condensation nuclei or as ice-nucleating particles (INPs). INPs are required for heterogeneous ice nucleation, which can occur via different modes—contact, immersion, condensation freezing, and deposition nucleation (Pruppacher & Klett, 2010; Young, 1993). Amongst these freezing modes, immersion freezing is thought to contribute significantly to the total ice crystal concentration at temperatures between 273 and 238K (Hande & Hoose, 2017). Here, we focus on this immersion freezing process, which occurs when VA particles are fully immersed in a cloud droplet and cool before freezing takes place (Vali et al., 2015).

VA refers to particles <2 mm in size, which are usually generated by brittle processes from a porous, crystal-bearing magma. At sufficiently high cooling rates, the individual fragments are composed of at least three phases, a glassy (=amorphous) matrix containing gas bubbles and crystals. The VA particles can frequently contain crystals of different phases and sizes (Dingwell et al., 2012).

VA can act as INP depending on temperature and relative humidity conditions of the atmosphere. Previous studies on the ice nucleation properties of VA particles obtained from different sources under both mixed-phase and cirrus cloud conditions have reported broadly different results (Durant et al., 2008; Fornea et al., 2009; Genareau et al., 2018; Gibbs et al., 2015; Hoyle et al., 2011; Jahn et al., 2019; Kulkarni et al., 2015; Mangan et al., 2017; Maters et al., 2019; Schill et al., 2015; Steinke et al., 2011). These studies have clearly established that VA particles can nucleate ice in the immersion freezing mode. Nevertheless, their ice nucleation activity (INA) at any given temperature can vary by up to five orders of magnitude, as shown in Figure 1. VA samples obtained from different eruptive episodes and different areas of a particular volcano can also vary remarkably in their ice nucleation abilities (Mangan et al., 2017; Schill et al., 2015), presumably due to differences in their physical and chemical properties. Currently, there is no clear explanation for the huge variability of the INA of VA (Figure 1). This contradicts the assumption that VA samples generally have comparable ice-nucleating properties (Durant et al., 2008). Some attempts have been made to link the INA of VA particles to their mineral and chemical compositions. For example, Genareau et al. (2018) studied five VA samples and found that the most ice active VA sample had a high K_2O and a low MnO content. Mangan et al. (2017) suggested that the INA of Soufrière Hills VA could be due to the presence of Na-feldspars. A more recent ice nucleation study of VA particles from Volcán de Fuego, Santiaguito, and Soufrière Hills volcanoes attributed their high freezing activity mainly to pyroxene crystals with a potential contribution from Ca- and Na-feldspars (Jahn et al., 2019). The presence of mineral phase(s) in a glassy or micro-crystalline matrix of VA samples can also provide a clue to their ice nucleation potential. Maters et al. (2019) demonstrated the importance of mineral phases in ice nucleation by showing that crystal-bearing VA samples are better INPs than their chemically equivalent, remelted and quenched, glassy, crystal-free equivalents. Further, they found that the most ice-active VA samples contained K-feldspar, Na-/Ca-feldspar, and/or pyroxene crystals, leading to the hypothesis that ice-active VA may originate most typically from magmas of felsic to intermediate composition that commonly crystallize those phases in abundance.

The Murray et al. (2012) ice nucleation parametrization for VA cloud-microphysics is based on only two samples and therefore neglects the extensive variability of VA properties from different eruptions and volcanoes (e.g., Vogel et al., 2017). Conclusions from previous studies were mostly based on measurements with only a few VA samples, except the recent work by Maters et al. (2019) who studied nine different VA sam-
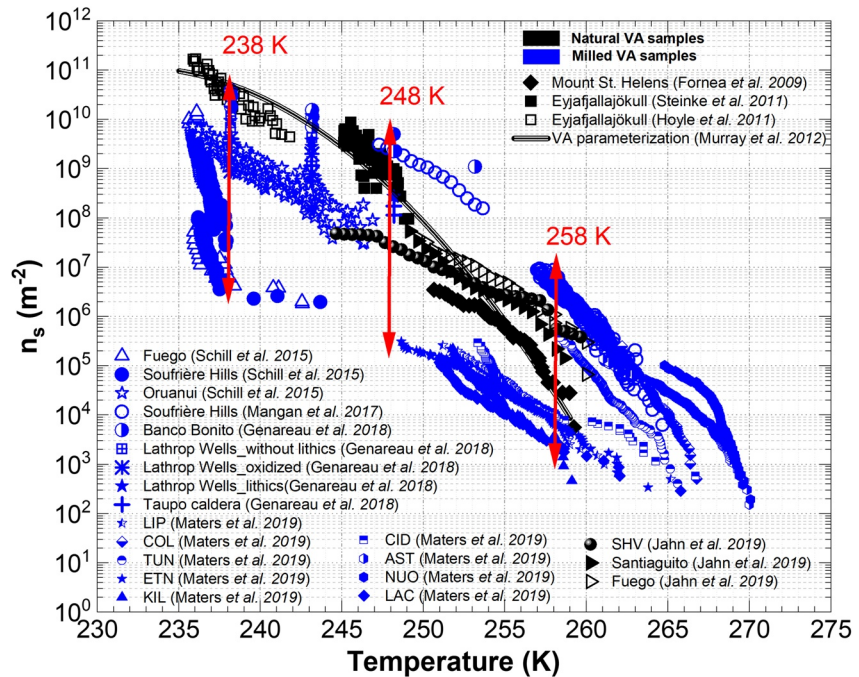
Figure 1. Summary of ice nucleation active site (INAS) densities and ice nucleation parameterization for volcanic ash (VA) in the immersion freezing mode. Data were extracted from relevant ice nucleation studies in the literature (Fornea et al., 2009; Schill et al., 2015; Mangan et al., 2017; Genareau et al., 2018; Jahn et al., 2019; Maters et al., 2019; Steinke et al., 2011; Hoyle et al., 2011). The double-head red arrows show variabilities in the ice nucleation properties of VA from different volcanoes at a given temperature in 10 K intervals (258K, 248K, and 238K). The parameterization shown on this figure was developed by Murray et al. (2012) from ice nucleation data of ash from two volcanoes–Mount St. Helens and Eyjafjallajökull. This figure was adapted and updated from Mangan et al. (2017).

ples. Given the variability of VA from a single volcano (Hornby at al., 2019), there is a clear need to investigate a wider range of VA in order to account for textural and chemical variabilities. To date, most studies have focused mainly on the bulk mineral composition of the VA samples, with no detailed consideration of the variability in VA particle-to-particle compositions. Mangan et al. (2017) performed cooling-rate dependent ice nucleation experiments with Soufrière Hills VA particles and observed no significant differences in their INA. They adapted their results to a modified ice nucleation stochastic model by Herbert et al. (2014) and predicted that Soufrière Hills VA has a strong particle-to-particle variability. Our understanding of particle-to-particle variability in VA compositions and how it might influence their INA is highly limited. For example, specific sites on feldspar minerals can trigger ice nucleation better than others (Holden et al., 2019; Kiselev et al., 2016).

In this study, we thus aim to explore the discrepancies in the INAs of VA particles and understand the factors that control their variable ice nucleation behavior. To achieve these objectives, we investigate the ice-nucleating properties of a wide range of VA samples ($n = 15$, 12 of the 15 samples are from different volcanoes) at experimental conditions relevant to mixed-phase clouds. For all samples, we characterized physicochemical properties (bulk chemical composition, abundance and type of minerals) in order to support the interpretation of the ice nucleation results. In addition, we investigated the particle-to-particle variability in the composition of the VA samples. By combining relevant ice nucleation results from the literature with our new data, we have developed a new, robust ice nucleation parameterization for immersion freezing by VA for use in aerosol-cloud microphysics and climate models. This article describes the experimental methods that we used, analyzes the physicochemical properties of the studied VA samples, and links these properties to the observed INA of the VA particles. We conclude our article by elaborating the potential atmospheric relevance of this study.

Table 1
Summary of VA Samples Investigated for Their Ice Nucleation Properties in the Immersion Freezing Mode

S/No.	VA source, country, and (continent)	Sample codes	Eruption period (dates) of the samples	Geographical locations of the source volcanoes [Lat, lon]	Volcanic classification[a]	SSA BET$_{Ar}$ (m²/g)	SSA geo (m²/g)	Pore volume (cm³/g)
1	Astroni, Italy (Europe)	AST	4000 BP	[40.827, 14.139]	Trachyphonolite	3	3.45	0.013
2	Chaiten, Chile (South America)	CHA	May, 2008	[−43.33, −72.47]	Rhyolite	~1	4.45	NA
3	Cordon Caulle, Argentina (South America)	COC	2011	[−40.59, −72.117]	Rhyolite	0.6	3.72	0.003
4	Da'Ure, Ethiopia (Africa)	DAU	2005	[12.595, 40.48]	Rhyolite	1.7	4.18	0.011
5	Etna, Italy (Europe)	ET1	1669	[37.748, 14.999]	Trachybasalt	0.3	3.63	0.003
6	Etna, Italy (Europe)	ET2	2016	[37.748, 14.999]	Trachybasalt	1.4	4.33	0.005
7	Mt. Kelud, Indonesia (Asia)	KEL	February, 2014	[−7.93, 112.308]	Basaltic Andesite	~1	4.53	0.005
8	Laacher See, Germany (Europe)	LAS[b]	13,000 BP	[50.25, 7.16]	Phonolite	~1	4.27	0.019
9	Mount St. Helens, USA (North America)	MSH	1982	[40.492, −121.508]	Dacite	~1	4.76	0.003
10	Pavlof, Alaska, USA (North America)	PAV	March, 2016	[55.417, −161.894]	Basaltic Andesite	~1	4.42	0.042
11	Mt. Sakurajima, Japan (Asia)	SA1	July, 2013	[31.59, 130.66]	Andesite	~	3.99	NA
12	Mt. Sakurajima, Japan (Asia)	SA2	July, 2013	[31.59, 130.66]	Andesite	~1	3.69	0.003
13	Tungurahua, Ecuador (South America)	TU1	February, 2014	[−1.467, −78.442]	Andesite	~1	4.50	0.007
14	Tungurahua, Ecuador (South America)	TU2[c]	February, 2014	[−1.467, −78.442]	Andesite	0.3	4.30	0.003
15	Unzen, Japan (Asia)	UNN	1992	[32.761, 130.299]	Dacite	~1	3.16	0.002

Note. The sample codes in column 3 are used throughout the text in this work. Volcanic classifications are based on the chemical information obtained from the characterization of these aerosol particles. Specific surface areas (SSA, BETAr measured for the bulk samples and Geo calculated for the filter samples), and pore volumes of the bulk samples are also reported.

[a]This classification is based on the silicon dioxide and the total alkali oxide compositions (see Figure 2 for more details). [b]This sample is also labeled as "LAC" or "LSB" in other studies, for example, Maters et al. (2019), Müller et al. (2020). [c]This sample is also labeled as "TUN" or "14TUN05" in other studies, for example, Maters et al. (2019), Müller et al. (2020).

2. Materials and Methods

2.1. Volcanic Ash Samples

Fifteen VA samples collected from 12 different volcanoes were studied. Details of the VA samples are given in Table 1 while the geographical distribution of the source volcanoes is shown in Figure 2a. Hereafter, all VA samples will be referred to in terms of the sample codes listed in Table 1. All VA samples were collected from relevant stratigraphic levels, preferentially deposited during the peak explosive activity. They were packed in buckets or plastic bags for transport to the laboratory where they were dried (110°C for 2 days) and then stored. Eleven samples were collected shortly after their eruptions. Additionally, we investigated four samples that had been collected substantially later than deposition but were included nevertheless due to the known or suspected impact of the eruption and/or their unique bulk rock composition: Mount St. Helens ash (MSH) was sampled 36 years after the eruption. The samples Astroni (AST), Etna (ET1), and Laacher See (LAS) correspond to eruptions which date back to 4000 BP (Before Present), 1669 AD (Anno Domini), and 13,000 BP, respectively. Two of the samples (ET1 and ET2) were obtained from Etna volcano but derive from two different eruptions (1669 and 2016 AD, respectively). We also examined two pairs of samples, each from the same eruption of this volcano, but from different sources: Sakurajima (SA1 and SA2) and Tungurahua (TU1 and TU2). All VA samples were dry sieved to ≤75 μm (*Analysette 3*, Fritsch® Germany)
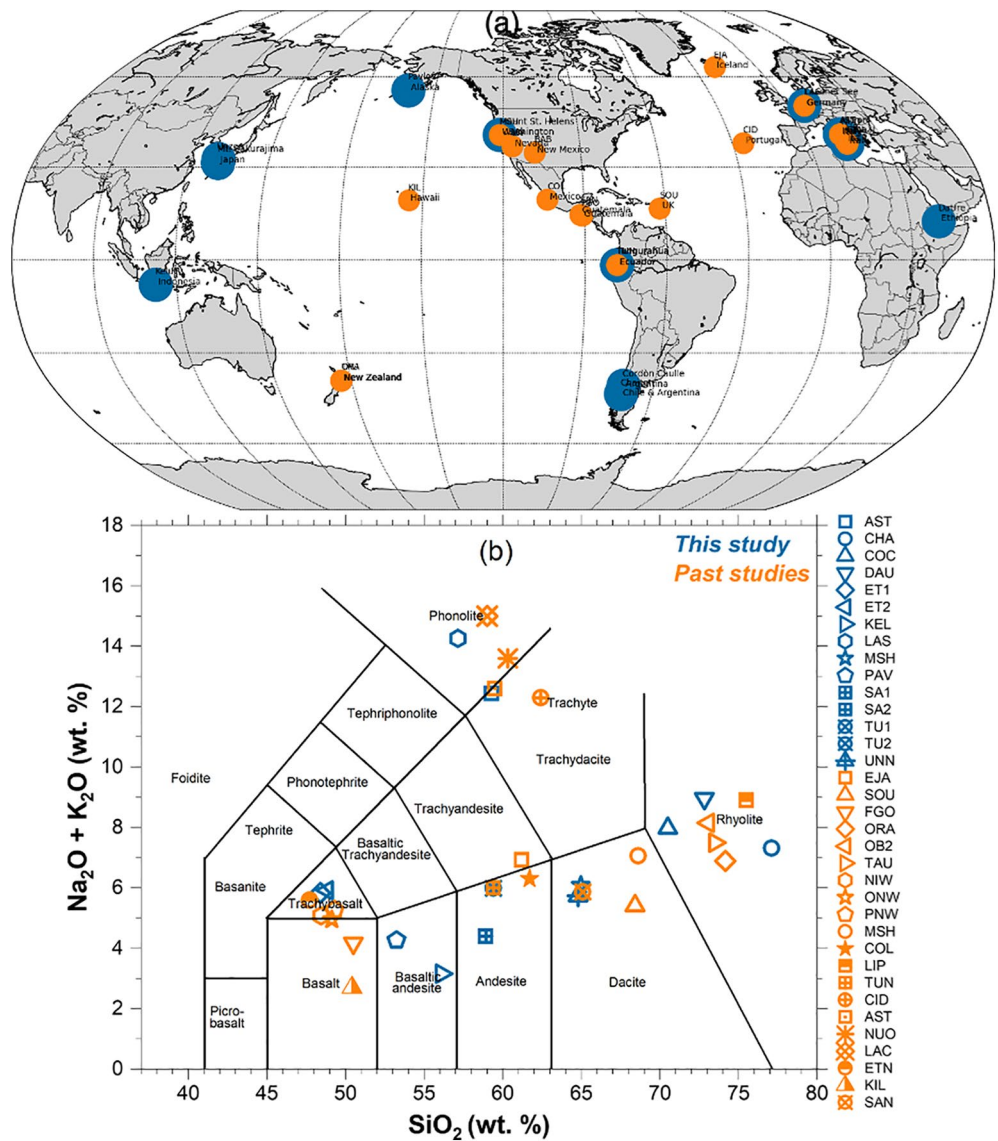
Figure 2. (a) A global map showing the locations of the source volcanoes from which the volcanic ash (VA) samples were collected for the ice nucleation studies. VA samples for the present work (blue dots) and the past studies (orange dots) are indicated on the map. Some data points are masked by others due to the low resolution of the map, for example, Sakurajima and Unzen are both in Japan. (b) A plot showing the classification of the VA samples following Le Maitre et al. (2013). The classification is based on the weight percentages of total alkali oxides (Na_2O and K_2O) and silicon dioxide (SiO_2) compositions of the VA samples. VA samples indicated by blue symbols are employed in the current study, while the orange symbols represent previous studies. In cases where two samples of the same volcano were studied, only one of them is indicated here.

except CHA, COC, DAU, and LAS, where the bulk samples already contained a sufficient amount of fine ash material. The ≤75 μm fraction (hereafter referred to as 'bulk') of the 11 sieved samples and the bulk of the four non-sieved samples were later used in sample characterization and ice nucleation experiments.

2.2. Characterization of the VA Particles

We characterized each of the VA samples in terms of the particles' morphology, specific surface area, porosity, as well as chemical and mineral compositions. The morphology of the samples was examined with an environmental scanning electron microscope (ESEM, FEI Quanta 650 FEG) at KIT as described in Umo et al. (2019) and with an analytical scanning electron microscope (ASEM, SU 5000 Schottky FE-SEM,
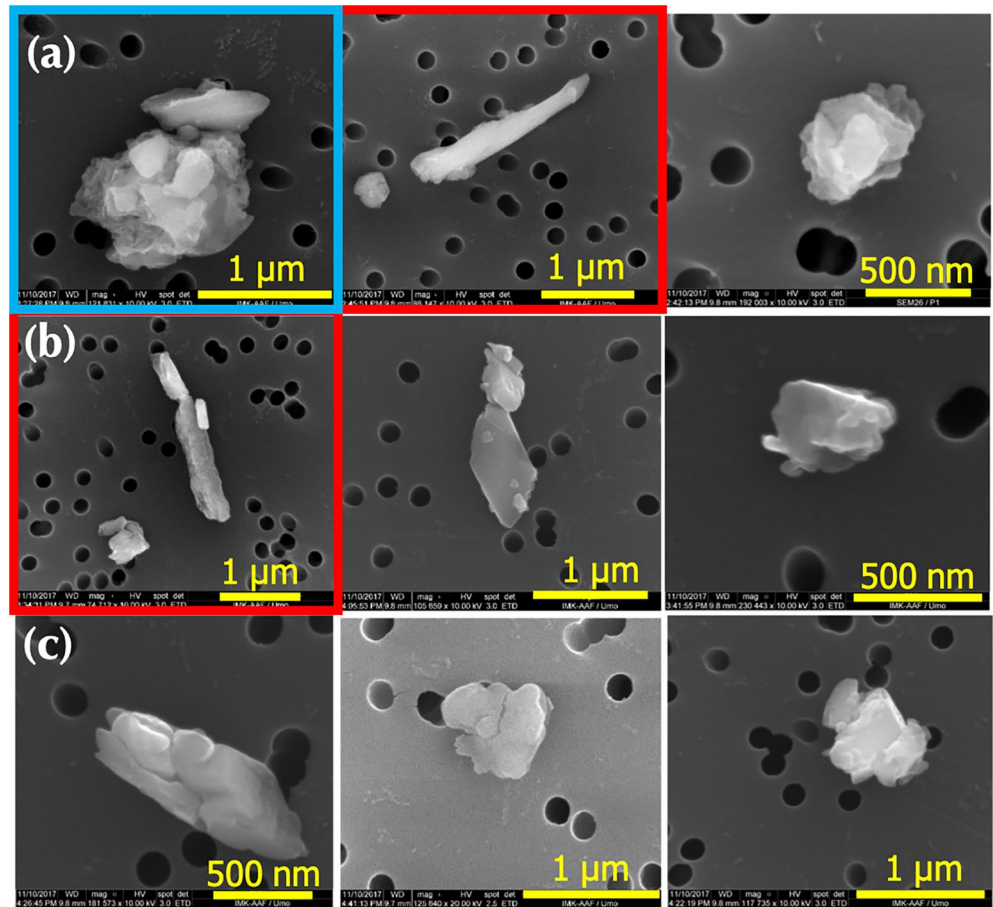
Figure 3. Images of representative volcanic ash (VA) particles obtained from an environmental scanning electron microscope (ESEM), showing their typical sizes and morphologies: (a) SA1, (b) TU1, and (c) PAV. The particles are generally <3 μm in size because they were passed through cyclones with a D_{50} cut-off ≈ 2.3 μm before entering the Aerosol Interaction and Dynamics in the Atmosphere (AIDA) chamber during the injection process. They were later collected on Nuclepore filters for imaging. Some particles were found to be rather elongated (red boxes), while some showed a high degree of inhomogeneity (blue box). More images are included in the Supporting Information (Figure S2).

HITACHI) at LMU. It should be noted that the VA particles that were imaged in this study were filter-collected from the AIDA chamber after the aerosolization process. Hence, the particles were in the same size range (≤3 μm) as those subjected to ice nucleation experiments in the AIDA chamber and INSEKT filter set-up (Sections 2.3.1 and 2.3.2). Representative images are presented in Figures 3 and S2.

The specific surface area (SSA) of the VA samples was measured following the standard Brunauer–Emmett–Teller (BET) method (Brunauer et al., 1938) with an Autosorb 1-MP Instrument (Quantachrome, Germany) using argon gas (Ar) as the adsorbent (Neimark et al., 1998; Thommes et al., 2006). We calculated the SSA BET_{Ar} from a 33-point Ar adsorption isotherm and the pore volume from a DFT/Monte Carlo method assuming a mixture of spherical and cylindrical pores on an oxygen-based substrate (Landers et al., 2013; Thommes et al., 2006). The results are presented in Table 1.

We also measured the chemical and mineral compositions of the bulk VA samples by X-ray fluorescence (XRF; XRF spectrometer MagiXPRO) and X-ray diffraction (XRD; D8 Advance Bruker-AXS, Germany), respectively. Both the XRF and the XRD techniques probe the entire bulk of the particles. For the XRF analysis, the bulk VA samples were fused and pressed into pellets before measurement. The secondary X-ray emitted was used to determine their elemental composition (Beckhoff et al., 2006; Johnson et al., 1999). The mineralogy and the amorphous and crystalline contents of the VA samples were analyzed by XRD. Specifically, a Cu K$\alpha_{1,2}$ radiation source equipped with a position-sensitive Lynxeye X-ray detector was used.
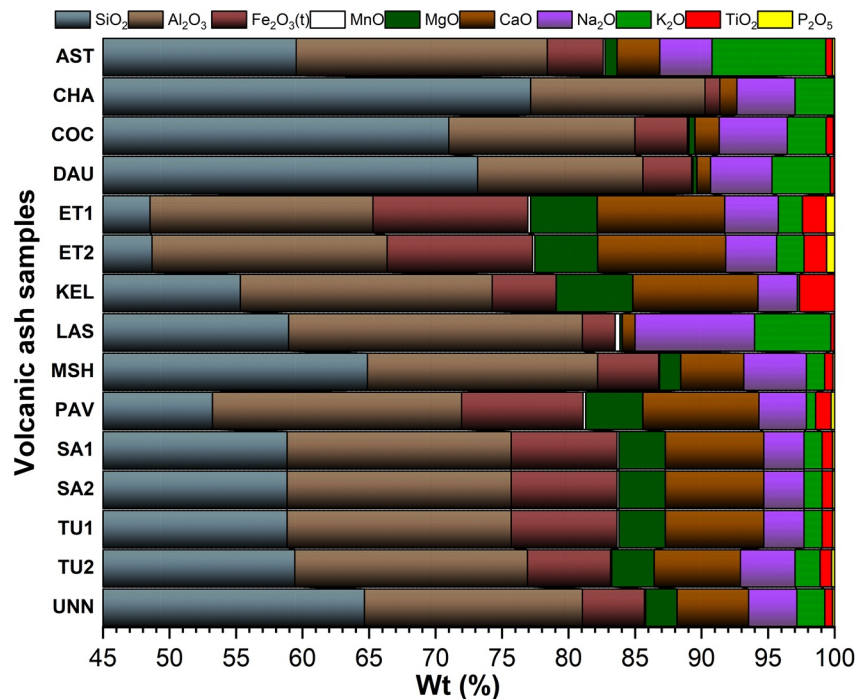
Figure 4. Chemical composition (wt %) of the volcanic ash (VA) samples investigated in this study as obtained from XRF analyses. Any group of chemical components <0.1 wt% was ignored in this plot. All samples contain more than 45 wt% of SiO$_2$, allowing the *x*-axis to be truncated at 45 wt% to better illustrate the minor components.

Rietveld refinement of the diffraction patterns (TOPAS 5.0 Software) was applied to obtain the mineralogy of the VA samples (An et al., 2018; Landers et al., 2013; Weidler et al., 1998). The uncertainty associated with our XRD measurements is within 1%–2%. The XRF results are shown in Figure 4 and Table S1, while the XRD data are presented in Figure 5.

2.3. Ice Nucleation Experiments

We employed two well-characterized set-ups for our VA ice nucleation studies: (a) the Aerosol Interaction and Dynamics in the Atmosphere (AIDA) aerosol and cloud simulation chamber, and (b) the Ice Nucleation SpEctrometer of the Karlsruhe Institute of Technology (INSEKT). The main difference between the instruments is that with AIDA, we employed a dry dispersion of the VA particles for the freezing experiments whereas with INSEKT, we used wet suspensions of the particles.

2.3.1. AIDA Cloud Chamber (Aerosol-to-Cloud Activation Method)

The AIDA aerosol and cloud simulation chamber is an 84 m³ aluminum vessel with 20 mm thick walls situated in a thermostatic housing. The chamber allows for an accurate control of temperature, pressure, and humidity for studying cloud formation processes. The thermostatic housing, coupled with a network of well-calibrated thermocouples mounted inside the chamber and on the chamber walls, ensures the effective control of the gas and the wall temperatures with an uncertainty of ±0.3 K (Möhler et al., 2006). Details on the development, calibration, and the operation of the AIDA chamber have been reported in Möhler et al. (2003), Wagner et al., (2016), Umo et al. (2019), and references therein. Here, we only briefly describe the experimental procedure and the employed measurement instruments. Before each individual ice nucleation experiment, the AIDA chamber was cleaned and filled with particle-free synthetic air. The background particle concentration in the chamber after the cleaning cycle was typically <0.01–0.05 particles per cm³. Thereafter, we injected the VA particles into the clean chamber using a rotating brush generator (RBG, RBG1000, PALAS GmbH, Germany) coupled with two cyclones that removed particles larger than ~3 μm in diameter; hence, the effective median diameter of the VA particles used in the experiments was ~0.8 μm (Figure 6). The number of VA particles at the start of the experiments were between 163 and 335 particles
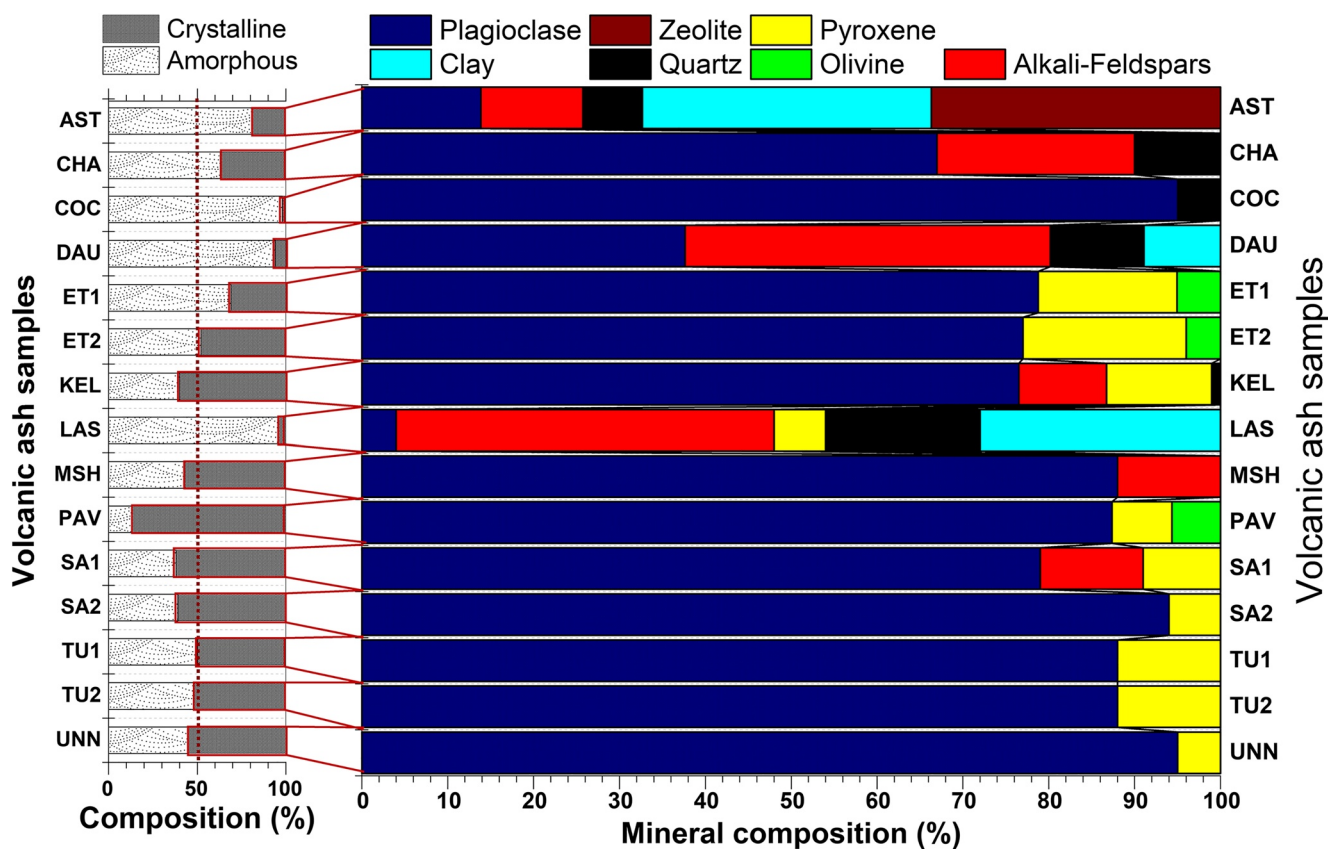
Figure 5. Mineralogy of the investigated volcanic ash (VA) samples. Percentages of the amorphous and crystalline components for each sample are shown on the left-hand side. Mineral compositions (wt. %) of the VA samples investigated in this study as obtained from XRD analyses and corrected with data from the XRF analyses are shown on the right-hand side. The principal mineral groups shown here were summed up from their sub-components as follows: Plagioclase [Anorthite, Labradorite, Andesine, and Oligoclase], Alkali-feldspars [Anorthoclase and Sanidine], and Pyroxene [Diopside and Pigeonite].

per cm^3. Hence, the activated fractions of all VA particles types tested were well above that of the background aerosol, thus making the latter insignificant for our experiments. In the chamber, a stainless-steel fan was constantly in operation to ensure an effective mixing of the aerosol particles in the chamber.

The size of the particles from the aerosolized VA samples was measured online with a combination of an aerodynamic particle sizer (APS; TSI GmbH, USA), and a scanning mobility particle sizer (SMPS; TSI GmbH, USA). The number concentration of particles in the AIDA chamber was measured with a condensation particle counter (CPC3010, TSI, USA).

We conducted freezing experiments by a controlled reduction of the chamber pressure. Expansion-cooling led to a reduction of the gas temperature by ~10 K compared to the starting temperature. This experiment mimics the ascent of moist air parcels in the atmosphere. The starting temperatures of our expansion cooling experiments were in the range from 258 to 239K. During cooling, the VA particles were first activated to cloud droplets, followed by the freezing of the subset of the cloud droplets that contained an ice-active VA particle. We measured the number and the size of the VA aerosol particles, activated cloud droplets, and nucleated ice particles with two sets of optical particle counters (OPCs; welas 2000, Palas GmbH, Germany). Optical size thresholds were used to differentiate between small-sized seed aerosol particles, medium-sized cloud droplets, and larger-sized ice crystals. In this way, we calculated the ratio of number of nucleated ice particles to the total number of aerosol particles activated at each temperature. From the ice particle number concentration (n_i), we calculated the ice nucleation active sites (INAS) density (n_s) of the VA particles following the scheme illustrated by Ullrich et al. (2017) as indicated in Equation 1. Basically, the n_s calculation involves the normalization of the ice nucleation crystal number concentration to the available surface area of the VA particles calculated from the aerosol size distribution measurements (Seinfeld &
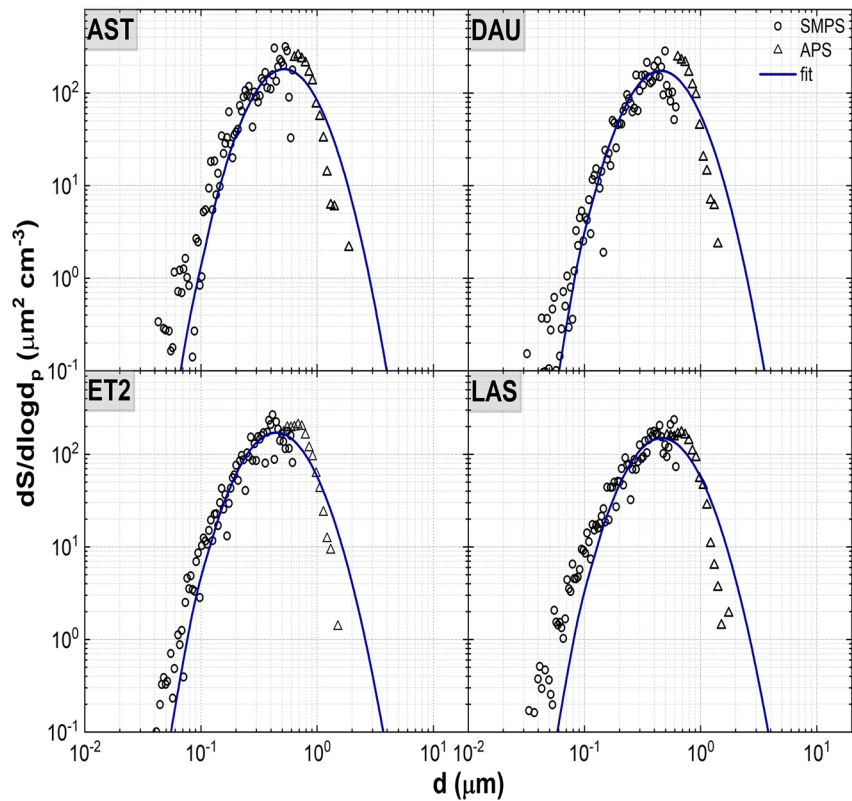
Figure 6. The surface area size distribution of four volcanic ash (VA) samples (AST, DAU, ET2, and LAS) as measured in the Aerosol Interaction and Dynamics in the Atmosphere (AIDA) chamber. The particle size was measured with scanning mobility particle sizer (SMPS) (open circles) and aerodynamic particle sizer (APS) (open triangles). The fit (blue line) combines data from both instruments. This fit was used to calculate the particles' geometrical surface area (S_{V_ae}) for the quantitative analysis of the ice nucleation data. For this fit combining the SMPS and APS data, we assumed a particle density of 2.75 g cm^{-3} and a dynamic shape factor of 1.2.

Pandis, 2006; Ullrich et al., 2017). This time-independent n_s value is useful for comparing the ice nucleation abilities of different aerosol particle types independently of the measurement techniques.

$$n_s(T) \approx \frac{n_i(T)}{S_{VA\_ae}} \qquad (1)$$

In Equation 1, n_s is the INAS density at temperature (T). $n_i(T)$ is the number concentration of nucleated ice crystals and S_{VA_ae} is the geometric surface area concentration of the VA particles. The full derivation of this equation can be found in Niemand et al. (2012) and Ullrich et al. (2017).

Before the expansion cooling experiment was started, the VA particles injected into the chamber were collected from the AIDA on 0.2 μm pore size Nuclepore filters® with a sampling flow rate of 10 L min^{-1} for 60 min. These filter-collected VA particles (hereafter referred to as 'filter samples') were then investigated using the cold-stage instrument INSEKT as described in the next section.

2.3.2. INSEKT (Suspension-to-Freezing Assay)

The suspension-to-freezing assay involves cooling aliquots of suspensions containing potential ice-nucleating particles until the aliquots freeze. INSEKT covers the freezing regime above ~255K, where AIDA is no longer sensitive enough to detect a very small amount of INPs. Therefore, INSEKT has an advantage here because it can access more INPs due to the large aliquot volume of 50 μL. In our experiments, we created suspensions both from the bulk VA samples and the filter samples collected from the AIDA chamber as described above. To make a suspension from the bulk VA samples, we added a known amount of the VA samples to a known volume of nanopure water and stirred effectively. For the filter samples, we washed off

the VA particles collected on the nuclepore filter with a known volume of nanopure water. Aliquots of these suspensions were then used in the INSEKT set-up to conduct the freezing experiments.

INSEKT is a type of a cold-stage freezing assay set-up, similar to the Colorado State University Ice Spectrometer, but custom-built in KIT, Germany (Dietel, 2017; Hill et al., 2014, 2016; Hiranuma et al., 2015; Schiebel, 2017; Schmitt, 2014). This set-up has four main parts–the cooling system, the suspension holders, the electronic visualization, and the data acquisition unit. The cooling system of INSEKT consists of a chiller that uses ethanol as a coolant and an aluminum block with conduits and wells for polymerase chain reaction (PCR) plates. Cooling is achieved by circulating chilled ethanol through the aluminum block, in which the PCR plates containing the aliquots are placed (Figure S1). The sample is illuminated with polarized light and a camera is placed over the PCR wells containing the suspensions to observe frozen and unfrozen aliquots per time by using changes in the light transmission intensity. The unfrozen aliquots are brighter than the frozen aliquots as seen by the camera. A customized control program records the temperature and the time at which each aliquot froze. For the bulk samples, the ice number concentration was obtained following the description by Vali (1971) (Equation 2). Equation 2 includes the cumulative nucleus spectrum, which is the cumulative number of nucleation sites per unit volume.

$$\frac{n_{ice}(T)}{n_{tot}} = 1 - \exp\left(-K(T)V\right), \tag{2}$$

where $n_{ice}(T)$ is the number of frozen aliquots, n_{tot} is the total number of aliquots, $K(T)$ is the cumulative nucleus spectrum, and V is the volume of the aliquots containing VA particles. The n_s was calculated by relating the cumulative nucleus spectrum to the surface area as described in Umo et al. (2015). For the bulk samples, the surface area was measured by the BET method (Section 2.2). For the filter samples probed with INSEKT, the number concentration of ice-active VA particles (C_{INP}) was obtained following the modified equation of Vali (1971, 2014, 2019), as illustrated by Kaufmann (2019) and shown in Equation 3,

$$C_{INP,corr} = \frac{V_{sol}}{V_{air}} \frac{d}{V_{well}} \ln\left(\frac{f_{l,w}}{f_l}\right), \tag{3}$$

where V_{sol} is the volume of nanopure water that was used in creating the suspension from the filter, V_{air} is the volume of the air sampled from AIDA, V_{well} is the volume of each well ($\sim$50 µL), and $f_{l,w}/f_l$ is the fraction of wells unfrozen. The background freezing signal of nanopure water was taken into account by subtracting its freezing spectrum of nanopure water from that of the cumulative freezing spectrum of the suspension with VA particles following the approach reported by Vali (1971, 2019). Three dilution steps were used–undiluted (1st), 15 times (2nd), 225 times (3rd).

We performed uncertainty analyses by adopting a simple linear error propagation using the errors associated with each of the parameters in Equations 2 and 3 following Vali (1971). In addition to the statistical error, the uncertainties associated with the various dilution steps are ±4%, ±5%, and ±7% for the 1st, 2nd, and 3rd dilutions, respectively (Kaufmann, 2019). For the filter samples, we calculated the INAS density, n_s, by normalizing the $C_{INP, corr}$ to the available surface area of the VA aerosol particles obtained by the geometric fit to the size distribution measured by the SMPS and APS instruments (Section 2.3.1). A similar approach of calculating n_s has been adopted in previous studies, for example, Hiranuma et al. (2015). The uncertainty associated with calculating the n_s is about ±20%.

2.4. Single Particle Analysis

In order to investigate the variability in the chemical composition of the particles within each VA sample, we analyzed individual particles using a computer-controlled environmental scanning electron microscope coupled with an energy-dispersive X-ray system (CC-ESEM/EDX). The ESEM instruments were FEI ESEM Quanta 200 FEG and 400 FEG FEI, the Netherlands, while the EDX detectors were EDAX Phoenix, EDAX, the Netherlands and X-Max 150 SDD, Oxford Instruments, UK, respectively. More details of this method have been previously described and discussed in Kandler et al. (2007, 2018). The VA particles used for this investigation were collected on transmission electron microscope (TEM) grids (Carbon films-S162N7, Plano GmbH, Wetzlar, Germany) with a micro inertial impactor (nozzle orifice diameter ~0.4 mm) from the AIDA

chamber. Therefore, we probed the same particles with sizes typically <3 μm that were also probed in the ice nucleation experiments in AIDA and INSEKT (filter samples).

The overall sampling time for each VA sample was ∼15 min to obtain an adequate concentration of single particles on the TEM grid (Kandler et al., 2007; Kandler, 2009). For each VA sample, over 2200 individual particles were investigated. We discarded all TEM grids that had fewer particles and those with damaged sampling foil. From the EDX analysis, the composition of the single particles was derived using the correction algorithms implemented in the EDX detector software (EDAX Genesis 5.331, Aztec 3.3b). The composition was quantified in atom percentage (%) for the major elements.

3. Results and Discussion

3.1. Morphology and Pore Volume of the VA Particles

The VA particles investigated in our study have different asymmetrical shapes, as shown by ESEM images of three representative VA samples (SA1, TU1, and PAV) in Figure 3. Further examples are shown in the Supporting Information (Figure S2). These images show that the particles were generally <2.5 μm in size as expected from our sampling procedure, even though some of them appear aggregated possibly due to interactions during sample collection. Aggregation of VA particles in nature is a well-established phenomenon, especially for particles <63 μm, and it is influenced by many factors including the eruption properties and relative humidity (Brown et al., 2012; Textor et al., 2006 and references therein; Mueller et al., 2016). Other studies observed similar morphological features for the respective VA samples imaged (e.g., Gibbs et al., 2015; Steinke et al., 2011). The morphologies of the VA particles in our study were not exclusively different from the shape features observed for typical mineral dust particles (e.g., Engelbrecht et al., 2016; Krueger et al., 2004). As morphology can influence the processing and transport of particles in the atmosphere (China et al., 2014; Dellino et al., 2012), it will be crucial to characterize size-dependent shape factors of the <2.5 μm sized VA particles in more detail in future studies.

The pore volumes of the VA samples ranged from 0.002 to 0.042 $cm^3 g^{-1}$ as shown in Table 1. For some of the VA samples (AST, DAU, LAS, and PAV), the pore volumes were an order of magnitude higher than others, which might be related to the eruption process or mechanism. VA particles can be highly fragmented and porous depending on the explosivity of the eruption, thereby affecting the shapes of the resulting particles (Dellino et al., 2012; Jordan et al., 2014; Scasso & Carey, 2005). It is important to note that porosity can impact the ice-nucleating behavior of particles at T < 235K via the so-called pore condensation and freezing (PCF) mechanism (David et al., 2019, 2020; Marcolli, 2017; Umo et al., 2019). For example, pore diameters of ∼2–9 nm have been suggested to be relevant for PCF (David et al., 2020; Wagner et al., 2016). Aside from porosity, altering the physical properties of particle surfaces of a mineral component (e.g., hematite) by milling can influence its INA (Hiranuma et al., 2014). Also, the type of chemical deposits on the surface of VA particles (Casas et al., 2019; Mueller et al., 2017) could potentially influence their ice nucleation activities. For example, anhydrite ($CaSO_4$) formed on milled VA surfaces by reaction with SO_2 at high temperatures may enhance INA, potentially by creating ice-active sites through a particular combination of surface chemistry and topography (Maters et al., 2020). Milling is expected to alter the chemical properties of VA surfaces by destroying features that have been generated by such ash-gas/aerosol interactions in the eruption plume (e.g., Delmelle et al., 2007; Maters et al., 2016).

3.2. Particle-to-Particle Variability

Heterogeneous ice nucleation is a surface phenomenon; hence, the variability in the VA particle compositions can influence their INA. We analyzed individual particles as described in Section 2.4 to understand the degree of variability between particles of the same VA sample. We collected a sufficient number of particles (>2200) for 7 samples (AST, COC, ET1, ET2, KEL, SA2, and TU2). The characteristic elemental ratios of single particles of the samples that we collected are shown in Figure 7 (ET2 is not shown because it was similar to ET1). We observed clear differences in the chemical composition of individual particles, indicating particle-to-particle variability, although the degree of variability differs for each sample. COC showed the least inter-particle-variation, while it was strongest for KEL and SA2. Apart from COC, also AST showed a lower degree of particle-to-particle variability compared to other samples. The small variability
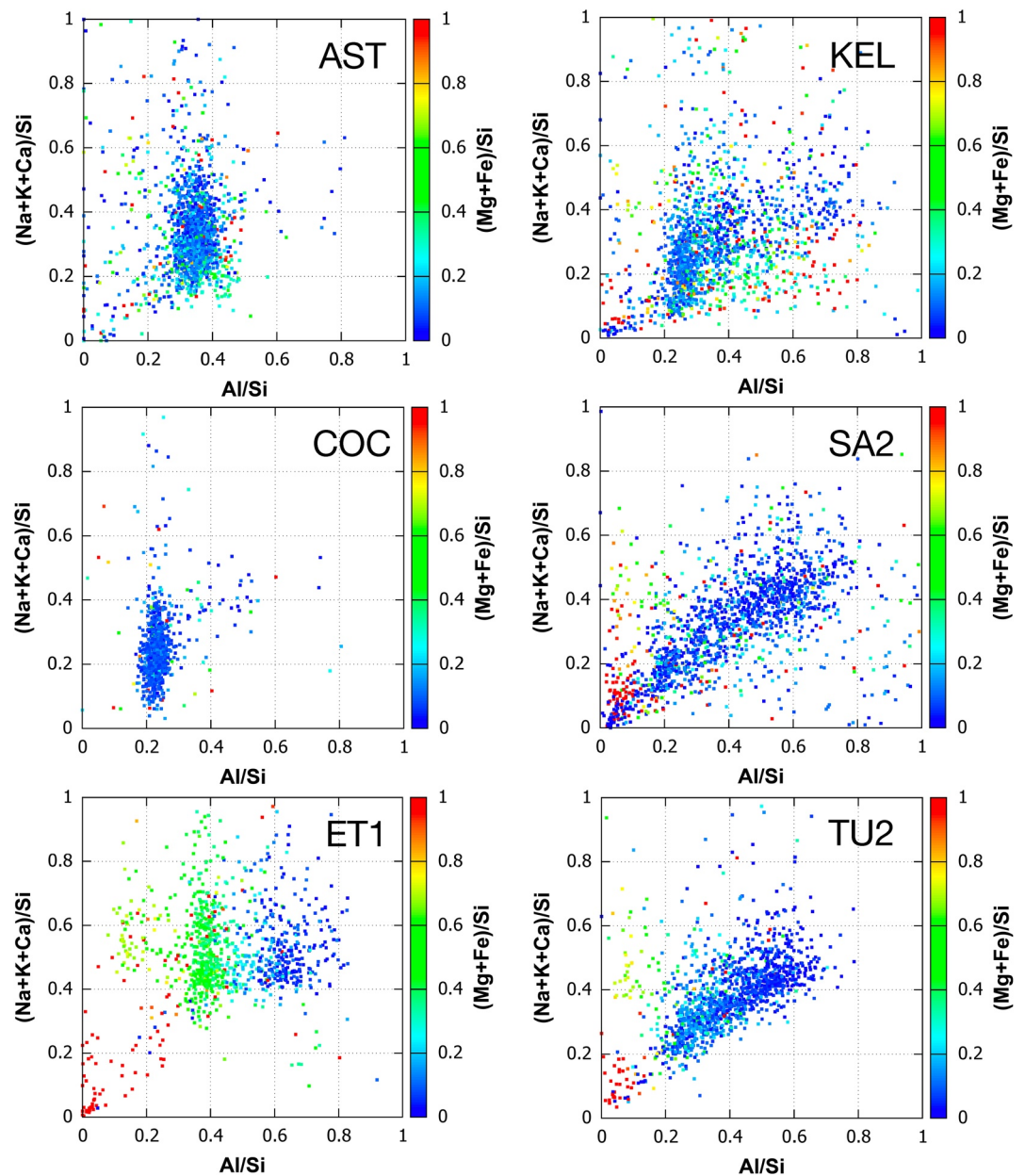
Figure 7. Characteristic elemental atomic ratios of the volcanic ash (VA) particles (<3 μm). Over 2200 individual particles were investigated for each sample shown here. The classification was done by considering the major components of the VA. Here, the (Na + K + Ca) group represents the chemical signature of the feldspar group (Mg + Fe) represents the pyroxene component, and (Al) represents mainly the aluminosilicate-based minerals. This plot illustrates the particle-to-particle variability in the elemental composition of the VA particles.

applies mainly to the Al contents. The higher contents of Fe, Ca, and K in AST and COC could explain the slightly higher interparticle variability. The chemical signature in the elemental distribution of ET1 is more heterogeneous and evenly distributed across the different elemental compositions than other VA samples. ET1 sample is also characterized with relatively high proportions of Mg- and Fe-containing particles. This indicates that the magma, which is the parent material of this tephra, may be Mg- and Fe-rich. The surface (∼≤10 nm) chemical composition of VA samples can influence the surface reactivity of such particles as well as the mineral phase partitioning on the particles' surface (Hornby et al., 2019; Hoshyaripour et al., 2015; Maters et al., 2016). ET1, TU2, and SA2 show different populations of particles with distinct

Figure 8. Ice nucleation active site (INAS) densities of VA particles as measured by Ice Nucleation SpEctrometer of the Karlsruhe Institute of Technology (INSEKT) (suspension-to-freezing assay technique). The measurements with the bulk VA particles are indicated by the filled symbols, while the data for the aerosolized VA particles collected on a filter are represented by open symbols and with an 'F' on the legend (e.g., SA1_F). Colors are assigned to each pri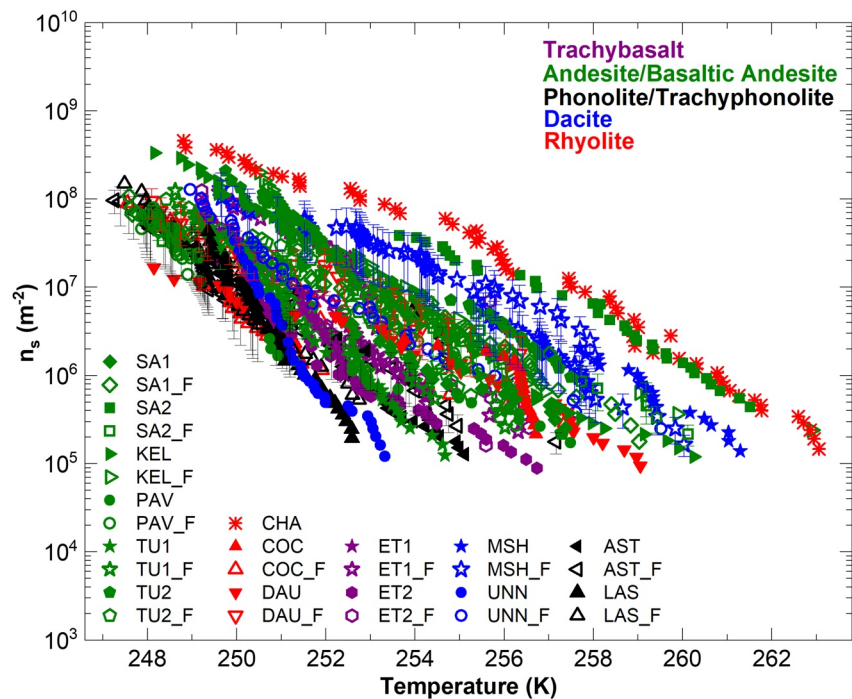mary class of the volcanic ash (VA) sample based on Le Maitre et al. (2013). Only some representative error bars are shown on the plot in order to not obscure the readability of the plot.

Mg + Fe-poor composition, which might point to different eruption phases or the inclusion of material not freshly erupted. KEL has in contrast a large, but continuous variation range.

The ice nucleation study by Mangan et al. (2017) suggested that the ice-nucleation behavior of Soufrière Hills (SOU) showed a strong particle-to-particle variability. Here, we used the elemental composition of the VA particles to evaluate the variability between particles. The results of our investigation confirm that some VA samples exhibit particle-to-particle variability; however, it is not entirely clear how this phenomenon can influence their ice nucleation behavior. From many studies, it is clear that particles trigger ice nucleation from the surface (e.g., Holden et al., 2019; Kiselev et al., 2016); hence, this variability can influence the INA of VA samples. It is important to understand the extent with which surface composition variability can contribute to the variability in VA ice nucleation activities. Mineral dust particles also show differences in their particle-to-particle compositions. A recent study has shown that the elemental ratio of natural mineral dust can differ with particle sizes (Kandler et al., 2018). It is possible that the differences in VA surface chemical compositions also vary with size. Therefore, understanding the role of particle size will be useful in attributing the potential influence of such variability to a particular size range.

Comparing the single particle analyses to the XRD data, COC showed the least variability and the lowest crystallinity (2%) (Figure 5). ET1, overall rich in Fe, shows a high Fe_2O_3(t) composition (11.6%) of bulk rock samples (XRF analysis) as well as high Fe-contents (19%) in pyroxene crystals (XRD data). Due to insufficient sample amount, LAS and PAV could not be analyzed. It is worth noting here that bulk measurements (XRF and XRD) agree with the sub-surface measurements of single particles.

3.3. Ice Nucleation Properties of the VA Particles

Volcanic ash samples nucleated ice in the immersion freezing mode in both the AIDA and the INSEKT measurements, as shown in Figures 8–10. Here, both filter and bulk results from the INSEKT set-up are
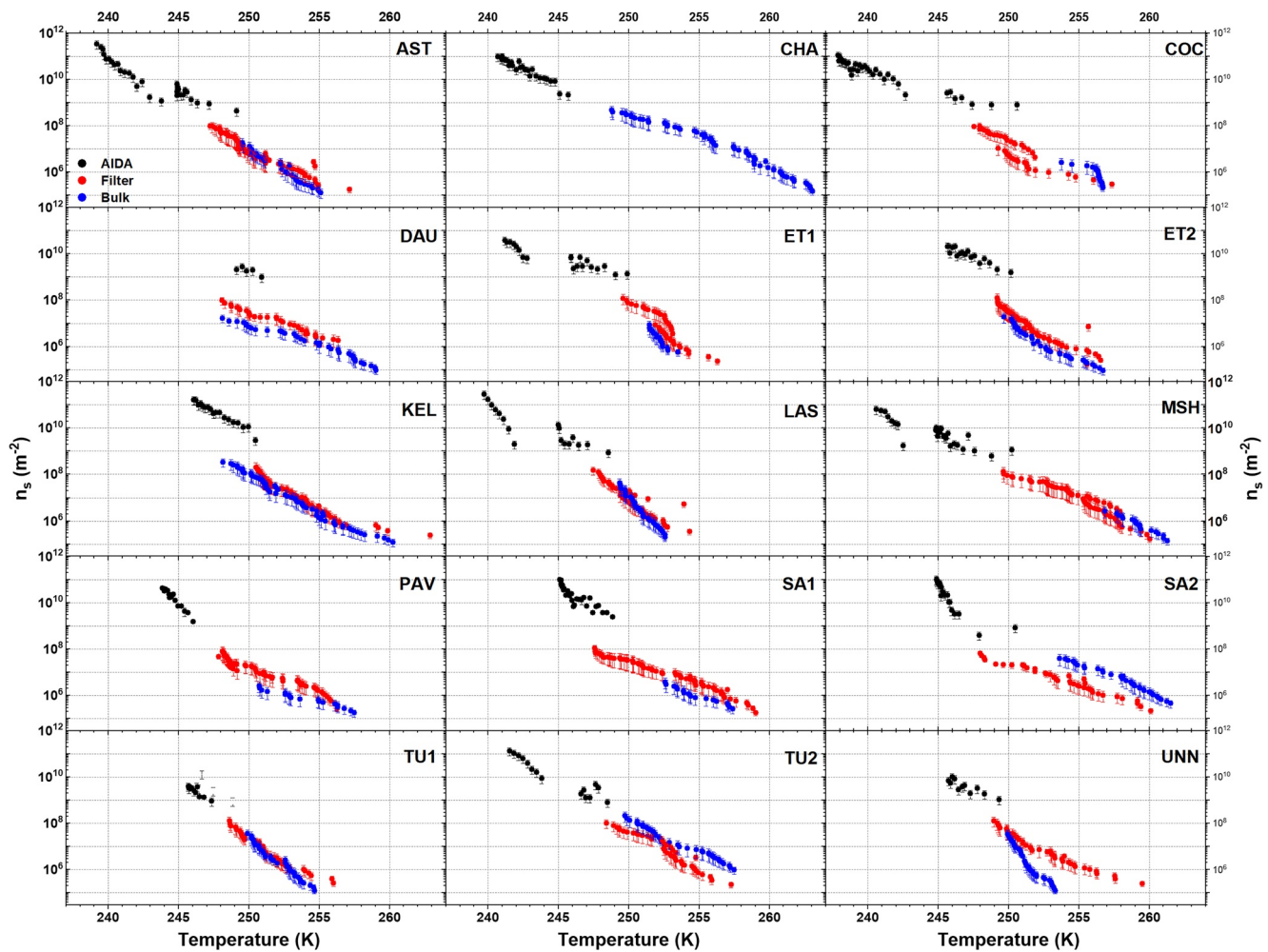
Figure 9. Ice nucleation active site (INAS) densities of 15 different volcanic ash (VA) samples investigated in this study. For each panel, the n_s from AIDA (black), INSEKT_filter (red) and INSEKT_bulk (blue) are shown. Some samples show Aerosol Interaction and Dynamics in the Atmosphere (AIDA) data corresponding to expansions that were carried out different start temperatures (e.g., AST, LAS, TU2, MSH, and others).

discussed. All VA samples investigated showed increasing n_s values with decreasing temperature (Figures 9 and 10). However, at the lower temperatures covered by the INSEKT measurements, the gradient of LAS is slightly steeper than others (Figures 8 and 9). This relative steepness is also shown in the lower temperature AIDA measurements. This indicates a relatively higher activity at both lower and higher temperatures, which may have been triggered by the presence of ice-active, evenly distributed unique sites in the particles. Particles with such properties trigger freezing within a narrower temperature range than those that have a less-uniform distribution of nucleation sites active over a broader range of temperatures. Some INPs such as illite and coal fly ash have also shown a steep increase of the n_s values within a narrow temperature regime around 254 K (Hiranuma et al., 2014; Umo et al., 2015).

For the INSEKT measurements, the n_s values of all VA samples span a range of 2.5 orders of magnitude at any given temperature from ∼248 to 258K. This underlines the high degree of variability in the ice-nucleation ability of different VA particles. Regarding previous ice nucleation measurements (Figure 1), we cannot rule out that instrument bias may have contributed to the observed variabilities in n_s, given that different measurement systems and sample handling methods were used. In our new measurements, however, where all the samples were treated in the same way and investigated with the same instrument, the variability in the IN behavior of the VA samples can only be related to the intrinsic particle properties. Previous studies have already linked INA variability of VA samples to variations in mineral compositions (Jahn et al., 2019; Maters et al., 2019; Schill et al., 2015). This sort of behavior is typical for INPs such as mineral
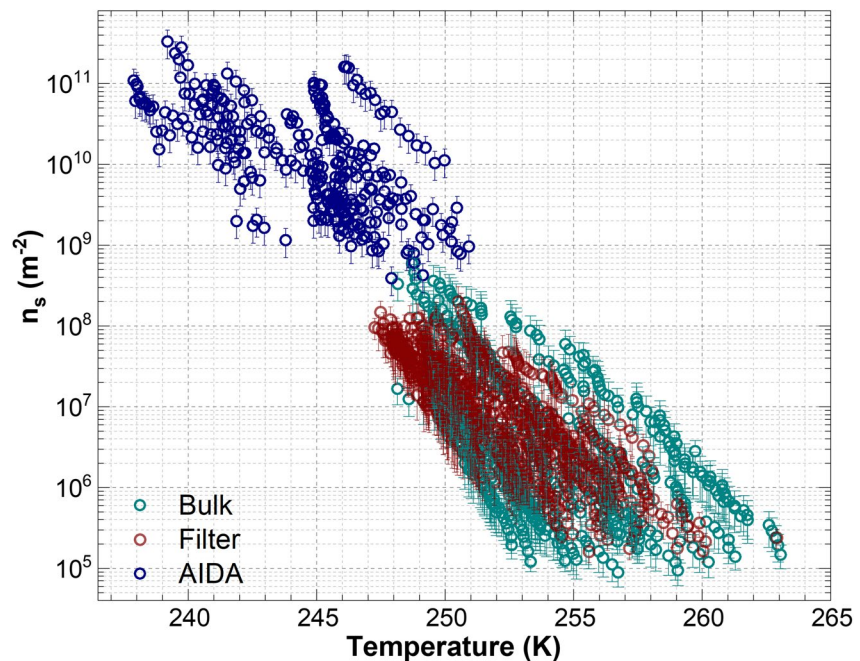
Figure 10. Comparison of the ice nucleation active site (INAS) densities of the volcanic ash (VA) particles from all employed techniques covering the full range of mixed-phase cloud temperatures. The data include AIDA experiments (blue), Ice Nucleation SpEctrometer of the Karlsruhe Institute of Technology (INSEKT) experiments using the filter samples collected from Aerosol Interaction and Dynamics in the Atmosphere (AIDA) (brown), and bulk VA particles (cyan).

dust collected from different regions in the world. For example, the differences observed in the INA of mineral dust particles have been attributed to mineral composition (Boose et al., 2016).

The results obtained from the AIDA cloud chamber experiments show that the VA particles were ice-active from 251 to 238K with $n_s \sim 10^9$ to 10^{11} m^{-2}, respectively (Figures 9 and 10). Most of the VA samples nucleated ice within a temperature range of 6K even with VA samples that showed ice activity in a temperature range of up to 10K in the higher temperatures. In contrast to the experiments with the INSEKT set-up (higher temperatures), AIDA results (lower temperatures) showed much less variation in their INA. KEL showed n_s values that were higher by about 1.2 orders of magnitude at lower temperatures (250–246K) compared with those from experiments at higher temperatures. Such ice-nucleating behavior is peculiar to INPs that have a high potential to exhibit pore condensation and freezing (Marcolli, 2014). It will be worth investigating if KEL exhibits such a freezing mechanism.

3.4. Ice Nucleation of Bulk Versus Filter Particles

We measured two sets of VA particles with our INSEKT set-up – (a) bulk particles as described in Section 2.1, and (b) VA filter samples. The main difference between the two investigations is the size range of the particles. For the bulk samples, the particles' diameter is ≤75 μm, whereas the filter-collected particles from the AIDA have sizes typically <2.5 μm as shown by the four representative size distribution measurements (AST, DAU, ET2, and LAS) in Figure 6. As apparent from Figures 8 and 9, and discussed in detail below, the n_s of a few of the VA samples showed discrepancies between the two sample sets (bulk and filter), whereas the majority did not. This suggests that a potential size-dependent effect on the INA of the VA particles is only visible in a small subset of the samples.

For 10 VA samples (AST, DAU, ET1, ET2, KEL, MSH, SA1, SA2, TU1, and TU2), the n_s values of both the bulk and the filter samples agreed within the uncertainty limits of the respective measurements (Figures S3a, 8 and 9). This indicates that the active sites driving the INA of these particles are evenly distributed in different size groups. Recently, a size-dependent study conducted with a single VA sample (FGO) showed

that no discrepancy was observed in the n_s values for particulate matter 2.5 μm ($PM_{2.5}$ μm), $PM_{\sim2.5-10}$ μm, $PM_{\sim10-37}$ μm, and $PM_{\sim37}$ μm (Jahn et al., 2019). Those authors did not observe any difference between sieved, ground, and FGO samples suspended in water for 24 h. Similarly, a study with the clay mineral kaolinite showed no size-dependent INA (Hartmann et al., 2016).

In contrast to the discussion above, UNN showed differences in INA signature between the bulk and filter samples (Figure S3b). This suggests that the distribution of active sites on these particles could be size-dependent. Sometimes aggregation can cause such differences in the n_s values. For example, Umo (2014) showed that aggregation in soot particles could limit the accessibility of water molecules to ice active sites in soot particles. However, in our measurements, we did not observe any effect of aggregation because for each sample set, there was a good overlap between the various dilution stages measured for each sample. In addition, the discrepancies observed in the measurements, even with the same instrument, further supports the interpretation that the variabilities observed in the ice nucleation abilities of VA studies in different set-ups (Figure 1) may not be due to instrumental artifacts.

Detailed mineralogical studies of VA ash samples showed size-dependent differences in bulk chemistry with variations in mineral/glass abundance (Hornby et al., 2019; Müller et al., 2019). Ice nucleation studies with size-segregated particles of montmorillonite, kaolinite, illite, and Arizona Test Dust (ATD) samples showed a weakly size-dependent ice nucleation efficiency in the immersion freezing mode, which became much stronger in the deposition nucleation mode (Lüönd et al., 2010; Welti et al., 2009). In another study, alumina powder particles showed a dependence of the INA on the particle size. Smaller alumina powder particles showed a lower degree of supercooling during the nucleation process than larger particles (Deville et al., 2010). A systematic size-dependent investigation of VA particles will be crucial in resolving the impact that size-dependent parameters may have on their INA. Some VA samples (TU2, COC, and PAV) studied here did not show a significant difference within the error estimation of our ice nucleation measurements.

Differences between the surface area determined by geometric calculations and by BET analysis could also contribute to the discrepancy in n_s across set-ups, as these two parameters can differ substantially (over an order of magnitude) for VA due to features such as surface roughness and texture (e.g., Riley et al., 2003). Unfortunately, a direct comparison of n_s values calculated from geometric versus BET surface area for the same experimental set-up is not possible, since we do not have information on the particle size distribution of the bulk samples and not enough material was collected for SSA BET_{Ar} measurement of the filter samples. However, the overall variability of the INA of all VA samples is ~3.5 orders of magnitude, which is far larger than the difference in n_s densities expected, even if an order of magnitude difference in geometric and BET surface area is assumed (Riley et al., 2003).

3.5. Wet Suspension Method Versus Dry Dispersion

We now turn to a close inspection of Figures 9 and 10, representing the combined n_s values of the VA particles investigated with INSEKT and AIDA. As described in Sections 2.3.1 and 2.3.2, INSEKT represents the wet suspension method and AIDA the dry dispersion method. When comparing the INAS densities of each VA sample from both INSEKT (bulk and filter samples) and AIDA measurements, it can be seen that most of the VA samples (10) showed a good agreement between both methods, meaning that there was a smooth transition between the slope of the INSEKT measurements at higher temperatures and the AIDA n_s traces recorded at lower temperatures (Figure S4a). In 4 cases (DAU, ET1, ET2, KEL, and SA1) however, we observed discrepancies between the techniques (Figure S4b), meaning that there was a stepwise increase of the n_s values by one order of magnitude in the overlap region of the AIDA and INSEKT datasets.

It is unclear why some samples showed agreement in the n_s values between both measurement techniques, whereas others did not. A study of ice nucleation of illite using both wet suspension and dry dispersion methods show a lower n_s for the wet suspension compared to the dry dispersion method (Hiranuma et al., 2015), thus revealing the same trend as observed for some of the VA samples. Similar differences between the wet suspension and dry dispersion results were also observed in a recent study on the INA of coal fly ash particles (Grawe et al., 2018) and complex plant-derived organic aerosol (Steinke et al., 2020). We suggest that wet chemistry (e.g., dissolved compounds) may contribute to the lower INA sometimes observed in the wet suspension methods, but this needs to be systematically investigated.

3.6. Effect of the Chemical Composition and Mineralogy on VA Ice Nucleation

The chemical composition of the studied VA samples is shown in Figure 4, where the major elements are plotted as their respective oxides. Elements of minor and trace concentrations <0.1% such as SO_3, Cr_2O_3, and NiO are not shown in Figure 4 but are included in Table S1. All VA samples comprise more than 48% SiO_2, with CHA having the largest amount (77%). The contents of Al_2O_3 vary from about 12% to 22%, making it the second most abundant component of the VA particles. The maximum values for MnO, TiO_2, and P_2O_5 were 0.35% (LAS), 2.70% (KEL), and 0.65% (ET1/ET2), respectively. MgO occurred in all the VA samples except in CHA. Two VA samples (AST and LAS) are phonolites and contain high concentrations of K_2O. Previously, chemical composition has been found to influence the INA of VA. Genareau et al. (2018) reported that the most ice active VA samples in the immersion freezing mode were found to contain the highest content of K_2O and the lowest content of MnO among the samples that they studied. Maters et al. (2019) also proposed an indirect relationship between ash chemical composition and INA, as related to a source magma of felsic to intermediate chemical composition which could yield ice-active K feldspar, Na/Ca feldspar, and/or pyroxene crystals in the resultant ash.

To investigate the influence of chemical composition on the INA of the VA samples studied here, we first used Pearson correlation analysis to study the correlation between SiO_2 and INA and between the total alkali (Na_2O and K_2O) content and INA. For this analysis, we used data from this study and the literature with a focus on natural and non-milled VA samples only. We performed the correlation analysis for n_s at different temperatures (T $\sim$ 258K, 253K, 248K, and 243K) as shown in Figure S5. No significant relationship was observed between either component (SiO_2 and the total alkali) and the n_s of the VA samples. To consider the correlation between all oxides and the INA of all samples at the same time, we employed a more robust statistical approach - principal component analysis (PCA). PCA is a non-dimensional analysis tool which uses an orthogonal transformation to convert a set of observed variables into a set of values of linearly uncorrelated variables called principal components (Tefas & Pitas, 2016; Wold et al., 1987). In our case, given N as the number of VA samples and n as the number of measured variables (x_n: n_s, SiO_2, Al_2O_3, Fe_2O_3(t), ...), a new set of ξ_n independent variables that are orthogonal to the preceding values was generated. A linear combination of the original variables measured in our study was obtained from Equation 4.

$$\xi_i = \sum_{j=1}^{n} a_{ij} x_j \tag{4}$$

The values of a_{ij} are such that the smallest number of the new variables are accounted for. The principal components (PC) are represented by ξ_i. PCA has a comparative advantage over Pearson correlation when many variables are concurrently considered (Aitchison, 1983; Wold et al., 1987).

For our PCA analyses, we used n_s values at a specified temperature (T_{ns}). For each temperature, we had n_s values from at least one of each of the three methods used in this study–AIDA, INSEKT (filter) and INSEKT (bulk). However, for cases where the n_s value was not available at the exact temperature, the mean value of the two n_s values bounding that temperature was used. The n_s values at lower temperatures were mainly from the AIDA data as indicated by the n_s range on Figures 9 and 10.

For most cases (13/15 or 86.7%) at higher temperatures, INSEKT (filter) and INSEKT (bulk) agree well, so that the PCA based on bulk mineralogy also should be valid for the particle measurements. For the two lower temperatures, in at least 70% of the cases shown in Figure 9, the extrapolation of the INSEKT (bulk/filter) data to lower temperatures would nicely overlap with the AIDA (particle) results.

The results of our PCA analyses by single value decomposition is presented in Figure S6. The same iso-temperatures as used in our Pearson correlation analyses were adopted. For T_{ns} = 258K, the two PCs (1 and 2) explained 82.89% of the variables. The proximity of the eigenvalues shown by the vector lines indicates the correlation between the mineral and n_s parameters. The green points with names of VA samples indicate the VA samples that contribute to the correlation. For every 5K interval - T_{ns} = 253K, 248K, and 243K, the PC_{tot} was 73.37%, 72.52%, and 75.84%, respectively. A strong correlation between Mg, Ca, Fe, and Ti oxides may reflect their co-occurrence in certain aluminosilicate or oxide minerals in the ash (e.g., pyroxenes, amphiboles, olivine). Overall, from the results of these statistics, we conclude that there is no correlation between chemical composition and the INA (n_s) of the VA samples analyzed. This result is in contrast to

the findings of Genareau et al. (2018) and Maters et al. (2019). However, an important difference in the VA samples across these studies may explain why these contrasting findings are not incompatible. It is well known that the bulk and surface composition of VA differ due to chemical alteration in the eruption plume (e.g., Delmelle et al., 2007). Therefore, in situations where natural VA samples have been tested as received (as in the present study), a lack of correlation between bulk composition and INA is not surprising, since water interacts with the distinct chemically altered surface during freezing experiments. However, in situations where VA samples have been milled before testing (e.g., Genareau et al., 2018; Maters et al., 2019), a correlation between bulk composition and INA may be revealed, since water interacts with the newly exposed surface more closely matching the bulk composition during freezing experiments. Therefore, we conclude that bulk chemical composition does not have primary importance in the INA of natural VA, and that the surface chemical composition may exert an influence on the INA of VA. A recent study on VA INA has shown that surface chemical composition can influence INA of milled VA samples (Maters et al., 2020). There might also be synergistic effects involving a complex interplay of surface chemical composition and other physicochemical properties in determining the INA of VA–this requires further investigation.

We also grouped the n_s of the VA samples into major groups based on their total alkali oxides (Na_2O and K_2O) and silica (SiO_2) contents. The major groups considered were trachybasalt, andesite/basaltic andesite, phonolite/trachyphonolite, dacite, and rhyolite. Figure 8 shows that variabilities in the INA exist even among the major groups of VA samples. This is consistent with the observation from our PCA analyses, that there is no direct correlation between VA ice nucleation abilities and Na_2O, K_2O, or SiO_2 contents.

Mineral compositions and phases play an important role in the INA of INPs (Atkinson et al., 2013; Kiselev et al., 2016; Maters et al., 2019, 2020). To understand the influence of mineralogy on the INA of the VA particles, we performed mineralogy analyses by XRD as described in Section 2.2. Figure 5 shows the percentage of crystalline and amorphous components as well as the mineral chemistry (in wt. %) of the crystalline phases. Some of the broad fields shown for some mineral phases are due to their capability of forming solid-state solutions: Plagioclase was found to range in composition from anorthite, through labradorite and andesine, to oligoclase. Alkali-feldspars range from anorthoclase to sanidine. Pyroxene ranges from diopside to pigeonite. All VA samples except PAV (13 wt. %) contained 38 wt. % glass or more (Figure 5). Amorphous fractions can vary widely among VA samples due to different priming of magma during ascent and cooling conditions during eruptions. Jahn et al. (2019) reported amorphous fractions of Fuego (20 wt.%), Santiaguito (75 wt.%), and SHV (76 wt.%) ash which are within the range of our samples (13%–96%). When comparing our data to crystallinities of VA from the same volcanoes as reported by Maters et al. (2019), we observed differences of up to 63.6% and sometimes close agreement to within 3.7%. It cannot be ruled out that this difference is due to the sample processing methods.

We investigated the relationship between the mineral compositions and the INA of the VA particles with PCA, as presented in Figure 11. At higher temperatures ($T_{ns} \sim 258$ and 253K), plagioclase has a weak link to the n_s. MSH, UNN and SA2 mainly contributed to the correlation of n_s with plagioclase (Figure 11). At lower temperatures ($T_{ns} = 248$ and 243K), the pyroxene content exhibits a stronger correlation with the n_s than does plagioclase. Thus, while plagioclase may be driving the ice nucleation at the higher temperature range, pyroxene appears to be controlling the INA at lower temperatures. We should state here that the mineralogical data with which we conclude the behavior of VA samples at lower temperatures were obtained from the bulk sample. The reason is we were unable to collect enough aerosolized VA samples from AIDA for XRD mineralogical analyses due to technical limitations. Although this was the case, we note that the aerosolized composition injected into AIDA is a subset of the bulk samples. For future studies, we aim at sampling in the same size range as employed in the ice nucleation experiments. Jahn et al. (2019) suggested that both pyroxene and feldspars may be responsible for the high INA of some of the VA samples that they reported; however, the mechanism of such synergy and quantitative assessment was lacking.

Quartz has been suggested to be the probable mineral responsible for the ice nucleation of Taupo Oruanui eruption VA ash (ORA) in the immersion mode (Schill et al., 2015). Generally, quartz is a minor component of most VA particles (Jahn et al., 2019; Mangan et al., 2017; Maters et al., 2019). Also, many ice nucleation studies of VA suggest that the feldspar component of VA may be driving its INA in the immersion freezing mode (Genareau et al., 2018; Jahn et al., 2019; Mangan et al., 2017; Maters et al., 2019; Schill et al., 2015). Feldspar minerals vary across a ternary composition and can be classified as K-rich "alkali"
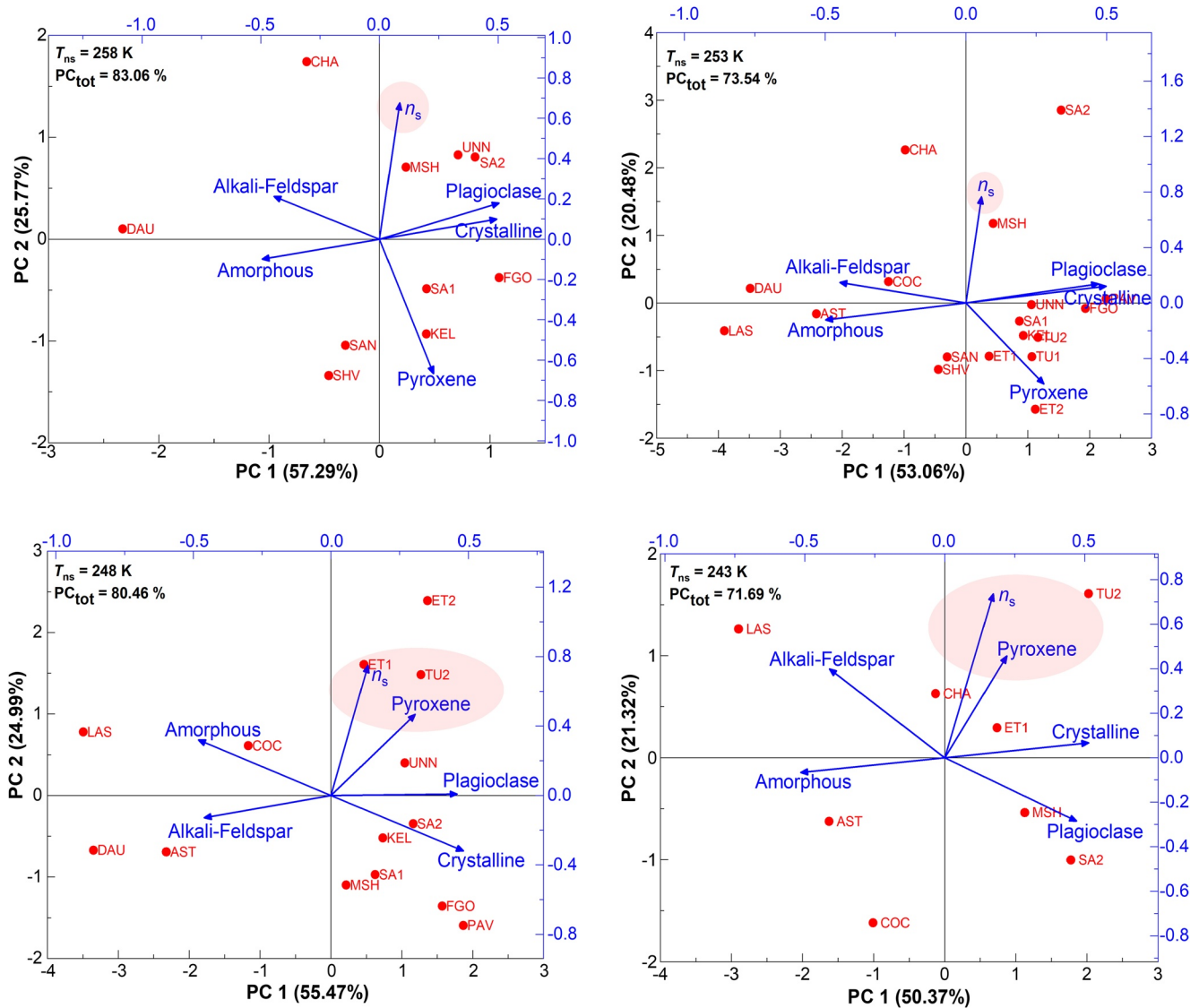
Figure 11. Principal component analyses of mineral compositions of the volcanic ash (VA) samples and their ice-nucleating abilities at different temperatures: T_{ns}~258K, 253K, 248K, and 243K. The shaded circles mark the most correlated parameter to the n_s which is considered in these analyses. The red dots show the different VA samples that were analyzed. The PC_{tot} indicates the percentage of components that were explained by the principal components ($PC1$ and $PC2$).

feldspar (orthoclase, sanidine) or Na-/Ca-rich "plagioclase" feldspar, from the Na endmember (albite) to the Ca endmember (anorthite). In our PCA study, plagioclase was the principal component in comparison with pyroxene that showed a dominant influence at lower temperatures. Combining the PCA results, the contributing VA samples and the mineral grouping as shown in Figure S7, it is obvious that this is a Ca-rich plagioclase. Although some VA minerals showed a relatively weak correlation with their INA at higher temperatures, no influence of K-feldspar was observed. Nevertheless, the question remains as to whether synergistic effects of the different mineral phases might enhance ice nucleation of mineral-based INPs. We recommend further investigations of these potential synergistic effects on INA capabilities of INPs.

3.7. Development of an Ice Nucleation Parameterization for the VA Particles

Atmospheric models that treat aerosol-cloud interactions can use data from laboratory and field INP measurements to investigate the importance of these INPs to cloud formation and climate. In such models, aerosol-independent ice nucleation parameterizations (e.g., DeMott et al., 2010) or aerosol-specific ice

Table 2
Summary of all Ice Nucleation Experiments of VA Particles in the Immersion Freezing Mode Cited in This Work

VA samples[a]	# of VA samples	Type of sample used	Instrumental set-up[b]	Temperature range (K)	INAS range (m^{-2})	Data used in the current parameterization	References
AST, CHA, COC, DAU, ET1, ET2, KEL, LAS, MSH, PAV, SA1, SA2, TU1, TU2, UNN	15	Natural	AIDA and INSEKT	264–236	$\sim10^5$–10^{11}	Yes	This study
FG2, SAN, SOU	3	Natural	CMU-CS	261–248	$\sim10^5$–10^9	Yes	Jahn et al., 2019
LIP, COL, TUN, CID, AST, NUO, LAC, ETN, KIL	9	Milled	µL-NIPI	270–248	$\sim10^2$–10^5	No	Maters et al., 2019
OB2, TAU, NIW, ONW, PINW	5	Milled	XDRS-CS	253–238	$\sim10^7$–10^{11}	No	Genareau et al., 2018
SOU	1	Milled	µL-NIPI and nL-NIPI	265–246	$\sim10^4$–10^{10}	No	Mangan et al., 2017
SOU, FGO, TAU	3	Milled	RS-CS	247–238	$\sim10^6$–10^{10}	No	Schill et al., 2015
SAT	1	Natural	LT-CS	252–235	N/A	No (incomplete information)	Gibbs et al., 2015
EJA	1	Natural	AIDA	249–244	$\sim10^8$–10^{10}	Yes	Steinke et al., 2011
EJA	1	Natural	IMCA/ZINC	240–238	$\sim10^{10}$–10^{11}	Yes	Hoyle et al., 2011
MSH	1	Natural	LT-CS	259–250	$\sim10^4$–10^6	Yes	Fornea et al., 2009
KIL, HUD, CRA, OGA, ATI, ORA	6	Natural	PD	260–250	N/A	No (very large particles $\sim 1,000\ \mu m$)	Durant et al., 2008

Note. For each study, information on the instrumental set-up, temperature range, and inferred INAS densities is given.
[a]Full names of the VA samples are given in Tables 1 and S1. [b]AIDA, Aerosol Interactions and Dynamics in the Atmosphere (aerosol/cloud simulation chamber); INSEKT, Ice Nucleation Spectrometer of the Karlsruhe Institute of Technology; CMU-CS, Carnegie Mellon University-Cold-Stage; RS-CS, X-ray Dispersive Raman Spectrometer - Cold-Stage; NIPI-µL, microliter-Nucleation by Immersed Particles Instrument; NIPI-nL, nanolitre-Nucleation by Immersed Particles Instrument; LT-CS, Linkam THMS600 Cold-Stage; IMCA/ZINC, Immersion Mode Cooling Chamber–Zurich ice Nucleation Chamber; PD, Peltier Devices.

nucleation parameterizations (e.g., Niemand et al., 2012; Ullrich et al., 2017) can be used. In addition, aerosol-specific parameterizations can be used to easily compare the mean INA of different aerosol types. From the results in our study, we developed an aerosol-specific parameterization for VA immersion freezing based on ice nucleation data from 19 different VA particles sampled globally, for use in aerosol-cloud interaction models. We combined the n_s data from our study with previous, well-documented ice nucleation experiments on natural VA samples in the literature (Table 2, Fornea et al., 2009; Hoyle et al., 2011; Jahn et al., 2019; Steinke et al., 2011). All experimental results from milled VA samples were excluded from our parameterization because milling can alter the INA of particles, for example, Niedermeier et al. (2011). The bulk n_s data of UNN was also excluded from the parameterization development. We made an exponential fit to this data set to obtain a n_s-T relationship that predicts the INA of the VA samples at any given temperature with an adjusted Pearson correlation 'r' value of −0.88118 (i.e., $R^2 = 0.78$) (Figure 12). The equation of the fit is given as:

$$log\left(n_s\right) = \alpha + \beta T \tag{5}$$

with $\alpha = 79.731 \pm 0.919$, $\beta = -0.288 \pm 0.004$, and T denoting the temperature in K, which is valid between 264 and 236K. The red transparent band in Figure 12 gives a 68.2% (±1 SD) upper and lower confidence limit for the VA n_s data. With the large number of samples, we now have a better basis to calculate a mean parameterization for the INA of the tephra; however, individual eruption material from certain volcanoes can still deviate from the parameterization in Figure 12. Note again that this new parameterization was
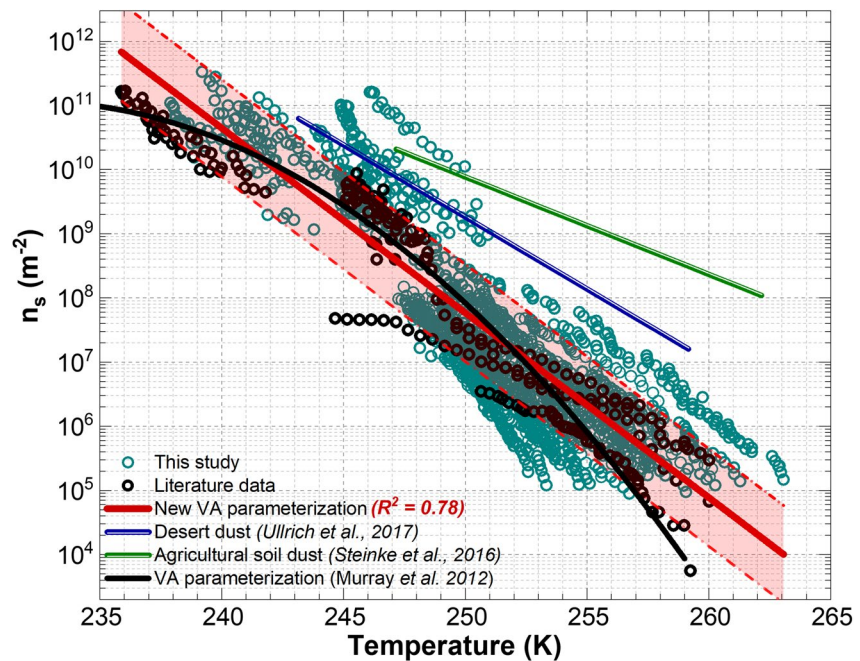
Figure 12. Parameterization of volcanic ash (VA) ice nucleation by immersion freezing and comparison of VA particle ice nucleation activities with other mineral INPs parameterizations. The new VA ice nucleation parameterization (thick red line) is given as $\log (n_s) = \alpha + \beta T$, with $\alpha = 79.73069 \pm 0.91924$, $\beta = -0.28785 \pm 0.00366$, and T denoting the temperature in K, being valid between 236 and 264K. The confidence band shows the 68.2% (± 1 SD) of the VA parameterization. The previous VA parameterization by Murray et al., 2012 is shown as the black line. Recent parameterizations of the ice nucleation active site (INAS) densities of agricultural soil dust (Steinke et al., 2016) and desert dust (Ullrich et al., 2017) are shown as comparison.

generated from 19 different VA samples, whereas the previous VA immersion freezing parametrization by Murray et al. (2012) was based on only 2 VA samples.

The Murray et al. (2012) parameterization compares relatively well with our new parameterization, however, there are differences at lower and higher temperatures (Figure 12). Above 257 K, the parameterization by Murray et al. (2012) drops below the 1 SD confidence interval of our current parameterization. We recommend that our new parameterization should be used to predict the mean contribution of VA particles to the global cloud ice budget in mixed-phase clouds.

3.8. Comparison of the VA Ice-Nucleating Properties With Other INPs

In this section, we compare the ice-nucleating properties of VA particles with those of other INPs (see Figure 12). In particular, we compare our parameterization line with the INAS densities reported for desert dust (Ullrich et al., 2017) and agricultural soil dust (Steinke et al., 2016). Figure 12 shows that VA particles are consistently 1.8 orders of magnitude less active than the desert dust particles in the temperature range from 259 to 243 K. Both parameterizations of the VA and desert dust have a similar gradient. The most active VA samples at least reach the mineral dust parameterization, but are clearly below the soil dust parameterization. Desert dust particles have different ice-nucleating properties depending on the chemical/ mineral compositions and their processing in the atmosphere (Boose et al., 2016). For example, the ice-nucleating ability of the desert dust surrogate Arizona Test Dust (ATD) was irreversibly lost when sulfuric acid was condensed on ATD particles (Sullivan et al., 2010). Conversely, Kanji et al. (2019) showed in a cloud chamber study that secondary organic aerosol (SOA)-coated desert dust and uncoated desert dust had no difference in their INAs under mixed-phase cloud conditions. This indicates that the atmospheric species that INPs such as desert dust or VA particles are exposed to have an important impact. Additionally, VA interacts with various gases and aerosols (e.g., SO_2, H_2SO_4, HCl) at high temperatures in the eruption plume, leading to chemical alteration of ash surfaces prior to dispersal in the wider atmosphere (e.g., Delmelle

et al., 2007, 2018). Maters et al. (2020) recently showed that high temperature ash-gas interaction can enhance or depress the INA of milled VA. In contrast, the influence of such ash-gas/aerosol interactions on the INA of natural VA remains unknown.

In addition, physical processing, such as milling of ATD particles, can also alter their ice-nucleating potential (Niedermeier et al., 2011; Reitz et al., 2011). In the case of VA, by destroying chemically altered surfaces imparted by ash-gas/aerosol interactions and exposing newly cleaved surfaces, milling is expected to modify its INA too. This is why we did not include studies that were performed with milled samples in our parameterization (Section 3.7). The INA of agricultural soil dust based on the Steinke et al. (2016) parameterization is much higher than that of the VA and desert dust. The difference gets more pronounced at the higher temperatures. For example, at 260K, the INA of agricultural soil dust is more than 3 orders of magnitude higher than that of the VA. Agricultural soil dust contains biogenic material which can trigger ice nucleation at higher temperatures starting from ~267K (Conen et al., 2011; Hill et al., 2014; O'Sullivan et al., 2014; Tobo et al., 2014), thereby explaining its superior INA compared to VA at these temperatures.

4. Atmospheric Relevance

VA particles influence atmospheric processes such as cloud formation by acting as INPs as demonstrated in this work and in previous studies (Durant et al., 2008). Field measurements of INP concentrations have shown a positive correlation with ongoing volcanic activities (Hobbs et al., 1971; Isono et al., 1959). Aside from the local impact that VA might have on clouds, ash particles can also undergo long-range transport in the atmosphere, and thereby have a global impact. Measurements have shown that Eyjafjallajökull ash particles were detected in Germany, which is over 2,200 km from the source (Seifert et al., 2011). Therefore, understanding the ice nucleation properties of VA particles is one of the crucial steps to reduce the current uncertainty associated with aerosol-cloud interactions (Boucher et al., 2013).

Another significant aspect of VA particles that is, often overlooked is their aging and transformation in the atmospheric environment. Currently, this is not well-understood for VA particles (Rose & Durant, 2011), and we suggest that more investigations should focus on the transformation and transportation pathways of these particles. Our study sheds light on a possible scavenging route of VA particles, which is ice formation. Quantifying the amount of VA particles involved in cloud formation will give more insight into how these particles are scavenged and transported in the atmosphere as well as help to predict the locations where the VA particles will be deposited. It is important that VA particles also experience physicochemical processing (e.g., oxidation, acidification) in the vertical eruption plume, laterally dispersed eruption cloud, and wider atmosphere during airborne transport, which likely lead to a modification in their intrinsic ice-nucleating abilities. These processes and their effect on ice nucleation by VA are still not well-understood and require further attention. Indeed, it is probable that the physicochemical properties of freshly emitted (airborne) VA ash particles differ from those of the deposited VA ash studied. To investigate this hypothesis, we suggest direct sampling of VA ash particles during primary suspension (e.g., possibly with drones), and evaluation of the properties of such particles, including comparison of their INA.

5. Conclusions

The ice nucleation properties of 15 VA samples were investigated under temperature and humidity conditions relevant for mixed-phase cloud formation. All VA samples were ice-active in the immersion freezing mode. Their ice nucleation efficiencies, calculated as the number of ice nucleation active sites per aerosol surface area, were $\sim 10^{5}$–10^{11} m^{-2} in the temperature range of 263–238K. This magnitude in n_{s} implies that VA particles can compete with natural mineral dust particles in cloud glaciation, especially in regions of enhanced volcanic activity where VA particles contribute a significant fraction of the atmospheric aerosol loading. No significant correlation was observed between the INA of natural VA particles and their bulk chemical compositions, contrary to what has been reported in some studies of milled VA samples. However, our results indicate that the VA ice nucleation activity is correlated with the plagioclase content at higher temperatures (>253K). At lower temperatures (<248K), the pyroxene content appears to become more important in driving the INA of the VA particles. Our results support previous studies that suggested that the

ice-nucleating abilities of VA might be controlled by their feldspar and pyroxene contents (Jahn et al., 2019; Mangan et al., 2017; Maters et al., 2019).

We clearly observed a particle-to-particle variability in the chemical compositions of the VA particles from the same sample. This observation supports the suggestions of Mangan et al. (2017). It is also in agreement with Hornby et al. (2019) who statistically quantified petrographic variations in 100–1,000s (hundreds to thousands) of individual clasts from several VA samples. Combining the ice nucleation data from this study and previous measurements, making up a total of 19 different natural VA samples from around the world, we have developed an improved ice nucleation parameterization for natural VA particles in the immersion freezing mode. This will be useful for aerosol-cloud modeling in estimating the potential contribution of VA particles to the global cloud ice budget.

Although our analyses show that the INA of VA correlates best with the presence of plagioclase and pyroxene crystals, more work is required to understand and quantify the contribution of other parameters, such as the surface properties of the particles. We also emphasize the need for size-selected characterization and ice nucleation measurements to understand how VA ice-nucleating abilities are partitioned between different size bins. Furthermore, we recommend that ice residues of VA particles should be investigated to understand the particle-to-particle variability in the INPs.

Data Availability Statement

The data presented in this work can be downloaded from the RADAR4KIT repository at https://dx.doi.org/10.35097/475 (Umo et al., 2021).

References

Aitchison, J. (1983). Principal component analysis of compositional data. *Biometrika*, *70*(1), 57–65. https://doi.org/10.1093/biomet/70.1.57

Alexander, D. (2013). Volcanic ash in the atmosphere and risks for civil aviation: A study in European crisis management. *International Journal of Disaster Risk Science*, *4*(1), 9–19. https://doi.org/10.1007/s13753-013-0003-0

An, L., Sasaki, T., Weidler, P. G., Wöll, C., Ichikuni, N., & Onishi, H. (2018). Local environment of strontium cations activating NaTaO$_3$ photocatalysts. *ACS Catalysis*, *8*(2), 880–885. https://doi.org/10.1021/acscatal.7b03567

Ansmann, A., Tesche, M., Groß, S., Freudenthaler, V., Seifert, P., Hiebsch, A., et al. (2010). The April 16, 2010 major volcanic ash plume over central Europe: EARLINET lidar and AERONET photometer observations at Leipzig and Munich, Germany. *Geophysical Research Letters*, *37*(13), L13810. https://doi.org/10.1029/2010GL043809

Atkinson, J. D., Murray, B. J., Woodhouse, M. T., Whale, T. F., Baustian, K. J., Carslaw, K. S., et al. (2013). The importance of feldspar for ice nucleation by mineral dust in mixed-phase clouds. *Nature*, *498*(7454), 355–358. https://doi.org/10.1038/nature12278

Ayris, P. M., & Delmelle, P. (2012). The immediate environmental effects of tephra emission. *Bulletin of Volcanology*, *74*(9), 1905–1936. https://doi.org/10.1007/s00445-012-0654-5

Beckhoff, B., Kanngießer, B., Langhoff, N., and Wedell, R. (2006). Handbook of practical X-ray fluorescence analysis. https://doi.org/10.1007/978-3-540-36722-2

Behnke, S. A., Thomas, R. J., McNutt, S. R., Schneider, D. J., Krehbiel, P. R., Rison, W., & Edens, H. E. (2013). Observations of volcanic lightning during the 2009 eruption of redoubt volcano. *Journal of Volcanology and Geothermal Research*, *259*, 214–234. https://doi.org/10.1016/j.jvolgeores.2011.12.010

Boose, Y., Welti, A., Atkinson, J., Ramelli, F., Danielczok, A., Bingemer, H. G., et al. (2016). Heterogeneous ice nucleation on dust particles sourced from nine deserts worldwide - Part 1: Immersion freezing. *Atmospheric Chemistry and Physics*, *16*(23), 15075–15095. https://doi.org/10.5194/acp-16-15075-2016

Boucher, O., Randall, D., Artaxo, P., Bretherton, C., Feingold, G., Forster, P., et al. (2013). *Clouds and aerosols. Climate change 2013: The physical science basis. Contribution of working group I to the fifth assessment report of the intergovernmental panel on climate change*. Cambridge University Press.

Brook, M., Moore, C. B., & Sigurgeirsson, T. (1974). Lightning in volcanic clouds. *Journal of Geophysical Research*, *79*(3), 472–475. https://doi.org/10.1029/jc079i003p00472

Brown, R. J., Bonadonna, C., & Durant, A. J. (2012). A review of volcanic ash aggregation. *Physics and Chemistry of the Earth*, *46*, 65–78. https://doi.org/10.1016/J.PCE.2011.11.001

Brunauer, S., Emmett, P. H., & Teller, E. (1938). Adsorption of gases in multimolecular layers. *Journal of the American Chemical Society*, *60*, 309–319. https://doi.org/10.1021/ja01269a023

Casadevall, T. J. (1994). *Volcanic ash and aviation safety: Proceedings of the first international symposium* (p. 450). US Geological Survey Bulletin.

Casas, A. S., Wadsworth, F. B., Ayris, P. M., Delmelle, P., Vasseur, J., Cimarelli, C., & Dingwell, D. B. (2019). SO$_2$ scrubbing during percolation through rhyolitic volcanic domes. *Geochimica et Cosmochimica Acta*, *257*, 150–162. https://doi.org/10.1016/j.gca.2019.04.013

China, S., Salvadori, N., & Mazzoleni, C. (2014). Effect of traffic and driving characteristics on morphology of atmospheric soot particles at freeway on-ramps. *Environmental Science & Technology*, *48*, 3128–3135. https://doi.org/10.1021/es405178n

Conen, F., Morris, C. E., Leifeld, J., Yakutin, M. V., & Alewell, C. (2011). Biological residues define the ice nucleation properties of soil dust. *Atmospheric Chemistry and Physics*, *11*(18), 9643–9648. https://doi.org/10.5194/acp-11-9643-2011

David, R. O., Fahrni, J., Marcolli, C., Mahrt, F., Brühwiler, D., & Kanji, Z. A. (2020). The role of contact angle and pore width on pore condensation and freezing. *Atmospheric Chemistry and Physics*, *20*(15), 9419–9440. https://doi.org/10.5194/acp-20-9419-2020

David, R. O., Marcolli, C., Fahrni, J., Qiu, Y., Sirkin, Y. A. P., Molinero, V., et al. (2019). Pore condensation and freezing is responsible for ice formation below water saturation for porous particles. *Proceedings of the National Academy of Sciences*, *116*(17), 8184–8189. https://doi.org/10.1073/PNAS.1813647116

Dellino, P., Gudmundsson, M. T., Larsen, G., Mele, D., Stevenson, J. A., Thordarson, T., & Zimanowski, B. (2012). Ash from the Ey-jafjallajökull eruption (Iceland): Fragmentation processes and aerodynamic behavior. *Journal of Geophysical Research*, *117*(1). https://doi.org/10.1029/2011JB008726

Delmelle, P., Lambert, M., Dufrêne, Y., Gerin, P., & Óskarsson, N. (2007). Gas/aerosol-ash interaction in volcanic plumes: New insights from surface analyses of fine ash particles. *Earth and Planetary Science Letters*, *259*(1–2), 159–170. https://doi.org/10.1016/j.epsl.2007.04.052

Delmelle, P., Wadsworth, F. B., Maters, E. C., & Ayris, P. M. (2018). High temperature reactions between gases and ash particles in volcanic eruption plumes. *Reviews in Mineralogy and Geochemistry*, *84*(1), 285–308. https://doi.org/10.2138/rmg.2018.84.8

DeMott, P. J., Prenni, A. J., Liu, X., Kreidenweis, S. M., Petters, M. D., Twohy, C. H., et al. (2010). Predicting global atmospheric ice nuclei distributions and their impacts on climate. *Proceedings of the National Academy of Sciences of the United States of America*, *107*(25), 11217–11222. https://doi.org/10.1073/pnas.0910818107

Deville, S., Maire, E., Lasalle, A., Bogner, A., Gauthier, C., Leloup, J., & Guizard, C. (2010). Influence of particle size on ice nu-cleation and growth during the ice-templating process. *Journal of the American Ceramic Society*, *93*(9), 2507–2510. https://doi.org/10.1111/j.1551-2916.2010.03840.x

Dietel, B. (2017). *Eisbildungsaktivität von atmosphärischem Aerosol über Zypern*. Karlsruher Institut für Technologie.

Dingwell, D. B., Lavallée, Y., & Kueppers, U. (2012). Volcanic ash: A primary agent in the Earth system. *Physics and Chemistry of the Earth*, *45–46*, 2–4. https://doi.org/10.1016/j.pce.2011.07.007

Durant, A. J., Shaw, R. A., Rose, W. I., Mi, Y., & Ernst, G. G. J. (2008). Ice nucleation and overseeding of ice in volcanic clouds. *Journal of Geophysical Research*, *113*(9). https://doi.org/10.1029/2007JD009064

Engelbrecht, J. P., Moosmüller, H., Pincock, S., Jayanty, R. K. M., Lersch, T., & Casuccio, G. (2016). Technical note: Mineralogical, chemical, morphological, and optical interrelationships of mineral dust re-suspensions. *Atmospheric Chemistry and Physics*, *16*(17), 10809–10830. https://doi.org/10.5194/acp-16-10809-2016

Fornea, A. P., Brooks, S. D., Dooley, J. B., & Saha, A. (2009). Heterogeneous freezing of ice on atmospheric aerosols containing ash, soot, and soil. *Journal of Geophysical Research*, *114*(D13), D13201. https://doi.org/10.1029/2009JD011958

Genareau, K., Cloer, S. M., Primm, K., Tolbert, M. A., & Woods, T. W. (2018). Compositional and mineralogical effects on ice nucleation activity of volcanic ash. *Atmosphere*, *9*(7), 238. https://doi.org/10.3390/atmos9070238

Gibbs, A., Charman, M., Schwarzacher, W., & Rust, A. C. (2015). Immersion freezing of supercooled water drops containing glassy volcanic ash particles. *GeoResJ*, *7*, 66–69. https://doi.org/10.1016/j.grj.2015.06.002

Grawe, S., Augustin-Bauditz, S., Clemen, H. C., Ebert, M., Eriksen Hammer, S., Lubitz, J., et al. (2018). Coal fly ash: Linking immer-sion freezing behavior and physicochemical particle properties. *Atmospheric Chemistry and Physics*, *18*(19), 13903–13923. https://doi.org/10.5194/acp-18-13903-2018

Gudmundsson, M. T., Thordarson, T., Hoskuldsson, A., Larsen, G., Bjornsson, H., Prata, F. J., et al. (2012). Ash generation and distribution from the April–May 2010 eruption of Eyjafjallajökull, Iceland. *Scientific Reports*, *2*. https://doi.org/10.1038/srep00572

Hande, L. B., & Hoose, C. (2017). Partitioning the primary ice formation modes in large eddy simulations of mixed-phase clouds. *Atmos-pheric Chemistry and Physics*, *17*(22), 14105–14118. https://doi.org/10.5194/acp-17-14105-2017

Hansen, J., Lacis, A., Ruedy, R., & Sato, M. (1992). Potential climate impact of Mount Pinatubo eruption. *Geophysical Research Letters*, *19*(2), 215–218. https://doi.org/10.1029/91GL02788

Hartmann, S., Wex, H., Clauss, T., Augustin-Bauditz, S., Niedermeier, D., Rösch, M., et al. (2016). Immersion freezing of kaolinite: Scaling with particle surface area. *Journal of the Atmospheric Sciences*, *73*(1), 263–278. https://doi.org/10.1175/JAS-D-15-0057.1

Herbert, R. J., Murray, B. J., Whale, T. F., Dobbie, S. J., & Atkinson, J. D. (2014). Representing time-dependent freezing behaviour in immer-sion mode ice nucleation. *Atmospheric Chemistry and Physics*, *14*(16), 8501–8520. https://doi.org/10.5194/acp-14-8501-2014

Hill, T. C. J., Demott, P. J., Tobo, Y., Fröhlich-Nowoisky, J., Moffett, B. F., Franc, G. D., & Kreidenweis, S. M. (2016). Sources of organic ice nucleating particles in soils. *Atmospheric Chemistry and Physics*, *16*(11), 7195–7211. https://doi.org/10.5194/acp-16-7195-2016

Hill, T. C. J., Moffett, B. F., DeMott, P. J., Georgakopoulos, D. G., Stump, W. L., & Franc, G. D. (2014). Measurement of ice nucleation-active bacteria on plants and in precipitation by quantitative PCR. *Applied and Environmental Microbiology*, *80*(4), 1256–1267. https://doi.org/10.1128/AEM.02967-13

Hiranuma, N., Augustin-Bauditz, S., Bingemer, H., Budke, C., Curtius, J., Danielczok, A., et al. (2015). A comprehensive laboratory study on the immersion freezing behavior of illite NX particles: A comparison of 17 ice nucleation measurement techniques. *Atmospheric Chemistry and Physics*, *15*(5), 2489–2518. https://doi.org/10.5194/acp-15-2489-2015

Hiranuma, N., Hoffmann, N., Kiselev, A., Dreyer, A., Zhang, K., Kulkarni, G., et al. (2014). Influence of surface morphology on the immer-sion mode ice nucleation efficiency of hematite particles. *Atmospheric Chemistry and Physics*, *14*(5), 2315–2324. https://doi.org/10.5194/acp-14-2315-2014

Hlodversdottir, H., Petursdottir, G., Carlsen, H. K., Gislason, T., & Hauksdottir, A. (2016). Long-term health effects of the Eyjafjallajökull volcanic eruption: A prospective cohort study in 2010 and 2013. *BMJ Open*, *6*(9), e011444. https://doi.org/10.1136/bmjopen-2016-011444

Hobbs, P. V., Fullerton, C. M., & Bluhm, G. C. (1971). Ice nucleus storms in Hawaii. *Nature Physical Science*, *230*(12), 90–91. https://doi.org/10.1038/physci230090a0

Holden, M. A., Whale, T. F., Tarn, M. D., O'Sullivan, D., Walshaw, R. D., Murray, B. J., et al. (2019). High-speed imaging of ice nucleation in water proves the existence of active sites. *Science Advances*, *5*(2), eaav4316. https://doi.org/10.1126/sciadv.aav4316

Hornby, A. J., Lavallée, Y., Kendrick, J. E., Rollinson, G., Butcher, A. R., Clesham, S., et al. (2019). Phase partitioning during fragmen-tation revealed by QEMSCAN Particle Mineralogical Analysis of volcanic ash. *Scientific Reports*, *9*(1). https://doi.org/10.1038/s41598-018-36857-4

Hoshyaripour, G. A., Hort, M., & Langmann, B. (2015). Ash iron mobilization through physicochemical processing in volcanic erup-tion plumes: A numerical modeling approach. *Atmospheric Chemistry and Physics*, *15*(16), 9361–9379. https://doi.org/10.5194/acp-15-9361-2015

Hoyle, C., Pinti, V., Welti, A., Zobrist, B., Marcolli, C., & Luo, B. (2011). Ice nucleation properties of volcanic ash from Eyjafjallajökull. *Atmospheric Chemistry and Physics*, *11*. https://doi.org/10.5194/acp-11-9911-2011

Isono, K., Komabayasi, M., & Ono, A. (1959). Volcanoes as a source of atmospheric ice nuclei. (Vol. 183, pp. 317–318). Nature Publishing Group. https://doi.org/10.1038/183317a0

Jahn, L. G., Fahy, W. D., Williams, D. B., & Sullivan, R. C. (2019). Role of feldspar and pyroxene minerals in the ice nucleating ability of three volcanic ashes. *ACS Earth and Space Chemistry*, *3*(4), 626–636. https://doi.org/10.1021/acsearthspacechem.9b00004

Johnson, D. M., Hooper, P. R., & Conrey, R. M. (1999). *XRF analysis of rocks and minerals for major and trace elements on a single low dilution Li-tetraborate fused bead* (pp. 843–867). JCPDS.

Jordan, S. C., Dürig, T., Cas, R. A. F., & Zimanowski, B. (2014). Processes controlling the shape of ash particles: Results of statistical IPA. *Journal of Volcanology and Geothermal Research*, *288*, 19–27. https://doi.org/10.1016/j.jvolgeores.2014.09.012

Kandler, K. (2009). *A miniature impactor for aerosol collection with emphasis on single particle analysis* (p. T092A04).

Kandler, K., Benker, N., Bundke, U., Cuevas, E., Ebert, M., Knippertz, P., et al. (2007). Chemical composition and complex refractive index of Saharan Mineral Dust at Izañã, Tenerife (Spain) derived by electron microscopy. *Atmospheric Environment*, *41*, 8058–8074. https://doi.org/10.1016/j.atmosenv.2007.06.047

Kandler, K., Schneiders, K., Ebert, M., Hartmann, M., Weinbruch, S., Prass, M., & Pöhlker, C. (2018). Composition and mixing state of atmospheric aerosols determined by electron microscopy: Method development and application to aged Saharan dust deposition in the Caribbean boundary layer. *Atmospheric Chemistry and Physics*, *18*(18), 13429–13455. https://doi.org/10.5194/acp-18-13429-2018

Kanji, Z. A., Sullivan, R. C., Niemand, M., DeMott, P. J., Prenni, A. J., Chou, C., et al. (2019). Heterogeneous ice nucleation properties of natural desert dust particles coated with a surrogate of secondary organic aerosol. *Atmospheric Chemistry and Physics*, *19*(7), 5091–5110. https://doi.org/10.5194/acp-19-5091-2019

Kaufmann, J. (2019). *Long-term measurements of ice nucleating particles in a boreal forest during the winter to spring transition*. Karlsruher Institut für Technologie.

Kiselev, A., Bachmann, F., Pedevilla, P., Cox, S. J., Michaelides, A., Gerthsen, D., & Leisner, T. (2016). Active sites in heterogeneous ice nucleation-the example of K-rich feldspars. *Science*, *355*(6323), 367–371. https://doi.org/10.1126/science.aai8034

Krueger, B. J., Grassian, V. H., Cowin, J. P., & Laskin, A. (2004). Heterogeneous chemistry of individual mineral dust particles from different dust source regions: The importance of particle mineralogy. *Atmospheric Environment*, *38*, 6253–6261. https://doi.org/10.1016/j.atmosenv.2004.07.010

Kulkarni, G., Nandasiri, M., Zelenyuk, A., Beranek, J., Madaan, N., & Devaraj, A. (2015). Effects of crystallographic properties on the ice nucleation properties of volcanic ash particles. *Geophysical Research Letters*, *42*. https://doi.org/10.1002/2015gl063270

Landers, J., Gor, G. Y., & Neimark, A. V. (2013). Density functional theory methods for characterization of porous materials. *Colloids and Surfaces A*, *437*, 3–32. https://doi.org/10.1016/j.colsurfa.2013.01.007

Le Maitre, R., Streckeisen, A., Zanettin, B., & Bas, M. L. (2013). Metamorphic rocks: A classification and glossary of terms: Recommendations of the international union of geological sciences subcommission on the systematics of metamorphic rocks. *Choice Reviews Online*, *45*(09), 45–4741. https://doi.org/10.5860/choice.45-4741

Lüönd, F., Stetzer, O., Welti, A., & Lohmann, U. (2010). Experimental study on the ice nucleation ability of size-selected kaolinite particles in the immersion mode. *Journal of Geophysical Research*, *115*(D14). https://doi.org/10.1029/2009jd012959

Mangan, T. P., Atkinson, J. D., Neuberg, J. W., O'Sullivan, D., Wilson, T. W., Whale, T. F., et al. (2017). Heterogeneous ice nucleation by Soufriere Hills volcanic ash immersed in water droplets. *PloS One*, *12*(1), e0169720. https://doi.org/10.1371/journal.pone.0169720

Marcolli, C. (2014). Deposition nucleation viewed as homogeneous or immersion freezing in pores and cavities. *Atmospheric Chemistry and Physics*, *14*(4), 2071–2104. https://doi.org/10.5194/acp-14-2071-2014

Marcolli, C. (2017). Pre-activation of aerosol particles by ice preserved in pores. *Atmospheric Chemistry and Physics*, *17*(3), 1595–1622. https://doi.org/10.5194/acp-17-1595-2017

Maters, E. C., Cimarelli, C., Casas, A. S., Dingwell, D. B., & Murray, B. J. (2020). Volcanic ash ice-nucleating activity can be enhanced or depressed by ash-gas interaction in the eruption plume. *Earth and Planetary Science Letters*, *551*, 116587. https://doi.org/10.1016/j.epsl.2020.116587

Maters, E. C., Delmelle, P., Rossi, M. J., Ayris, P. M., & Bernard, A. (2016). Controls on the surface chemical reactivity of volcanic ash investigated with probe gases. *Earth and Planetary Science Letters*, *450*, 254–262. https://doi.org/10.1016/j.epsl.2016.06.044

Maters, E. C., Dingwell, D. B., Cimarelli, C., Müller, D., Whale, T. F., & Murray, B. J. (2019). The importance of crystalline phases in ice nucleation by volcanic ash. *Atmospheric Chemistry and Physics*, *19*, 5451–5465. https://doi.org/10.5194/acp-19-5451-2019

Minnis, P., Harrison, E. F., Stowe, L. L., Gibson, G. G., Denn, F. M., Doelling, D. R., & Smith, W. L. (1993). Radiative climate forcing by the Mount Pinatubo eruption. *Science*, *259*(5100), 1411–1415. https://doi.org/10.1126/science.259.5100.1411

Möhler, O., Field, P. R., Connolly, P., Benz, S., Saathoff, H., Schnaiter, M., et al. (2006). Efficiency of the deposition mode ice nucleation on mineral dust particles. *Atmospheric Chemistry and Physics*, *6*, 3007–3021. https://doi.org/10.5194/acp-6-3007-2006

Möhler, O., Stetzer, O., Schaefers, S., Linke, C., Schnaiter, M., Tiede, R., et al. (2003). Experimental investigation of homogeneous freezing of sulphuric acid particles in the aerosol chamber AIDA. *Atmospheric Chemistry and Physics*, *3*(1), 211–223. https://doi.org/10.5194/acp-3-211-2003

Mueller, S. B., Ayris, P. M., Wadsworth, F. B., Kueppers, U., Casas, A. S., Delmelle, P., et al. (2017). Ash aggregation enhanced by deposition and redistribution of salt on the surface of volcanic ash in eruption plumes. *Scientific Reports*, *7*(1), 1–9. https://doi.org/10.1038/srep45762

Mueller, S. B., Kueppers, U., Ayris, P. M., Jacob, M., & Dingwell, D. B. (2016). Experimental volcanic ash aggregation: Internal structuring of accretionary lapilli and the role of liquid bonding. *Earth and Planetary Science Letters*, *433*, 232–240. https://doi.org/10.1016/J.EPSL.2015.11.007

Müller, D., Hess, K. U., Kueppers, U., & Dingwell, D. B. (2020). Effects of the dissolution of thermal barrier coating materials on the viscosity of remelted volcanic ash. *American Mineralogist*, *105*(7), 1104–1107. https://doi.org/10.2138/am-2020-7334

Müller, D., Kueppers, U., Hess, K. U., Song, W., & Dingwell, D. B. (2019). Mineralogical and thermal characterization of a volcanic ash: Implications for turbine interaction. *Journal of Volcanology and Geothermal Research*, *377*, 43–52. https://doi.org/10.1016/j.jvolgeores.2019.04.005

Murray, B. J., O'Sullivan, D., Atkinson, J. D., & Webb, M. E. (2012). Ice nucleation by particles immersed in supercooled cloud droplets. (Vol. 41, p. 6519). Royal Society of Chemistry. https://doi.org/10.1039/c2cs35200a

Neimark, A. V., Ravikovitch, P. I., Grün, M., Schüth, F., & Unger, K. K. (1998). Pore size analysis of MCM-41 type adsorbents by means of nitrogen and argon adsorption. *Journal of Colloid and Interface Science*, *207*(1), 159–169. https://doi.org/10.1006/JCIS.1998.5748

Niedermeier, D., Hartmann, S., Clauss, T., Wex, H., Kiselev, A., Sullivan, R. C., et al. (2011). Experimental study of the role of physicochemical surface processing on the inability of mineral dust particles. *Atmospheric Chemistry and Physics*, *11*(21), 11131–11144. https://doi.org/10.5194/acp-11-11131-2011

Niemand, M., Möhler, O., Vogel, B., Vogel, H., Hoose, C., Connolly, P., et al. (2012). A particle-surface-area-based parameterization of immersion freezing on desert dust particles. *Journal of the Atmospheric Sciences*, *69*(10), 3077–3092. https://doi.org/10.1175/JAS-D-11-0249.1

O'Sullivan, D., Murray, B. J., Malkin, T. L., Whale, T. F., Umo, N. S., Atkinson, J. D., et al. (2014). Ice nucleation by fertile soil dusts: Relative importance of mineral and biogenic components. *Atmospheric Chemistry and Physics*, *14*(4), 1853–1867. https://doi.org/10.5194/acp-14-1853-2014

Prata, A. J. (2009). Satellite detection of hazardous volcanic clouds and the risk to global air traffic. Natural Hazards (Vol. 51, pp. 303–324). Springer Netherlands. https://doi.org/10.1007/s11069-008-9273-z

Pruppacher, H. R., & Klett, J. D. (2010). *Microphysics of clouds and precipitation*. Springer.

Reitz, P., Spindler, C., Mentel, T. F., Poulain, L., Wex, H., Mildenberger, K., et al. (2011). Surface modification of mineral dust particles by sulphuric acid processing: Implications for ice nucleation abilities. *Atmospheric Chemistry and Physics*, *11*(15), 7839–7858. https://doi.org/10.5194/acp-11-7839-2011

Riley, C. M., Rose, W. I., & Bluth, G. J. S. (2003). Quantitative shape measurements of distal volcanic ash. *Journal of Geophysical Research*, *108*(B10). https://doi.org/10.1029/2001jb000818

Robock, A. (2000). Volcanic eruptions and climate. *Reviews of Geophysics*, *38*(2), 191–219. https://doi.org/10.1029/1998RG000054

Rose, W. I., & Durant, A. J. (2009). Fine ash content of explosive eruptions. *Journal of Volcanology and Geothermal Research*, *186*(1–2), 32–39. https://doi.org/10.1016/j.jvolgeores.2009.01.010

Rose, W. I., & Durant, A. J. (2011). Fate of volcanic ash: Aggregation and fallout. *Geology*, *39*(9), 895–896. https://doi.org/10.1130/focus092011.1

Scasso, R. A., & Carey, S. (2005). Morphology and formation of glassy volcanic ash from the August 12-15, 1991 eruption of Hudson Volcano, Chile. *Latin American Journal of Sedimentology and Basin Analysis*, *20*(1), 3–20.

Schiebel, T. (2017). *Ice nucleation activity of soil dust aerosols*. Karlsruhe Institute of Technology.

Schill, G. P., Genareau, K., & Tolbert, M. A. (2015). Deposition and immersion-mode nucleation of ice by three distinct samples of volcanic ash. *Atmospheric Chemistry and Physics*, *15*(13), 7523–7536. https://doi.org/10.5194/acp-15-7523-2015

Schmitt, T. (2014). *Homogeneous freezing of water droplets and its dependence on droplet size*. Karlsruhe Institute of Technology.

Seifert, P., Ansmann, A., Groß, S., Freudenthaler, V., Heinold, B., Hiebsch, A., et al. (2011). Ice formation in ash-influenced clouds after the eruption of the Eyjafjallajökull volcano in April 2010. *Journal of Geophysical Research*, *116*, D00U04. https://doi.org/10.1029/2011JD015702

Seinfeld, J. H., & Pandis, S. N. (2006). *Atmospheric chemistry and physics : From air pollution to climate change/John H. Seinfeld and spyros N. Pandis* (2nd ed.). John Wiley.

Steinke, I., Funk, R., Busse, J., Iturri, A., Kirchen, S., Leue, M., et al. (2016). Ice nucleation activity of agricultural soil dust aerosols from Mongolia, Argentina, and Germany. *Journal of Geophysical Research*, *121*(22), 13559–13579. https://doi.org/10.1002/2016JD025160

Steinke, I., Hiranuma, N., Funk, R., Höhler, K., Tüllmann, N., Umo, N. S., et al. (2020). Complex plant-derived organic aerosol as ice-nucleating particles-more than the sums of their parts? *Atmospheric Chemistry and Physics*, *20*, 11387–11397. https://doi.org/10.5194/acp-20-11387-2020

Steinke, I., Möhler, O., Kiselev, A., Niemand, M., Saathoff, H., Schnaiter, M., et al. (2011). Ice nucleation properties of fine ash particles from the Eyjafjallajokull eruption in April 2010. *Atmospheric Chemistry and Physics*, *11*(24), 12945–12958. https://doi.org/10.5194/acp-11-12945-2011

Sullivan, R. C., Petters, M. D., DeMott, P. J., Kreidenweis, S. M., Wex, H., Niedermeier, D., et al. (2010). Irreversible loss of ice nucleation active sites in mineral dust particles caused by sulphuric acid condensation. *Atmospheric Chemistry and Physics*, *10*, 11471–11487. https://doi.org/10.5194/acp-10-11471-2010

Tefas, A., & Pitas, I. (2016). Principal component analysis. *Intelligent Systems*. https://doi.org/10.1201/b14674-171

Textor, C., Graf, H. F., Herzog, M., Oberhuber, J. M., Rose, W. I., & Ernst, G. G. J. (2006). Volcanic particle aggregation in explosive eruption columns. Part II: Numerical experiments. *Journal of Volcanology and Geothermal Research*, *150*, 378–394. https://doi.org/10.1016/j.jvolgeores.2005.09.008

Thommes, M., Smarsly, B., Groenewolt, M., Ravikovitch, P. I., & Neimark, A. V. (2006). Adsorption hysteresis of nitrogen and argon in pore networks and characterization of novel micro- and mesoporous silicas. *Langmuir*, *22*(2), 756–764. https://doi.org/10.1021/la051686h

Tobo, Y., Demott, P. J., Hill, T. C. J., Prenni, A. J., Swoboda-Colberg, N. G., Franc, G. D., & Kreidenweis, S. M. (2014). Organic matter matters for ice nuclei of agricultural soil origin. *Atmospheric Chemistry and Physics*, *14*(16), 8521–8531. https://doi.org/10.5194/acp-14-8521-2014

Ulfarsson, G. F., & Unger, E. A. (2011). Impacts and responses of icelandic aviation to the 2010 Eyjafjallajökull volcanic eruption. *Journal of the Transportation Research Board*, *2214*(1), 144–151. https://doi.org/10.3141/2214-18

Ullrich, R., Hoose, C., Möhler, O., Niemand, M., Wagner, R., Höhler, K., et al. (2017). A new ice nucleation active site parameterization for desert dust and soot. *Journal of the Atmospheric Sciences*, *74*(3), 699–717. https://doi.org/10.1175/JAS-D-16-0074.1

Umo, N. S. (2014). *Ice nucleation by combustion products at conditions relevant to mixed-phase clouds*. University of Leeds.

Umo, N. S., Murray, B. J., Baeza-Romero, M. T., Jones, J. M., Lea-Langton, A. R., Malkin, T. L., et al. (2015). Ice nucleation by combustion ash particles at conditions relevant to mixed-phase clouds. *Atmospheric Chemistry and Physics*, *15*(9), 5195–5210. https://doi.org/10.5194/acp-15-5195-2015

Umo, N. S., Silas, N., Wagner, R., Ullrich, R., Kiselev, A., Saathoff, H., et al. (2019). Enhanced ice nucleation activity of coal fly ash aerosol particles initiated by ice-filled pores. *Atmospheric Chemistry and Physics*, *19*(13), 8783–8800. https://doi.org/10.5194/acp-19-8783-2019

Umo, N. S., Ullrich, R., Maters, E. C., Steinke, I., Benker, N., Höhler, K., et al. (2021). Data to: The influence of chemical and mineral compositions on the parameterization of immersion freezing by volcanic ash particles, *Journal of Geophysical Research*. https://doi.org/10.35097/475

Vali, G. (1971). Quantitative evaluation of experimental results an the heterogeneous freezing nucleation of supercooled liquids. *Journal of the Atmospheric Sciences*, *28*(3), 402–409. https://doi.org/10.1175/1520-0469(1971)028<0402:qeoera>2.0.co;2

Vali, G. (2014). Interpretation of freezing nucleation experiments: Singular and stochastic; sites and surfaces. *Atmospheric Chemistry and Physics*, *14*(11), 5271–5294. https://doi.org/10.5194/acp-14-5271-2014

Vali, G. (2019). Revisiting the differential freezing nucleus spectra derived from drop-freezing experiments: Methods of calculation, applications, and confidence limits. *Atmospheric Measurements Technics*, *12*, 1219–1231. https://doi.org/10.5194/amt-12-1219-2019

Vali, G., DeMott, P. J., Möhler, O., & Whale, T. F. (2015). Technical note: A proposal for ice nucleation terminology. *Atmospheric Chemistry and Physics*, *15*(18), 10263–10270. https://doi.org/10.5194/acp-15-10263-2015

Vogel, A., Diplas, S., Durant, A. J., Azar, A. S., Sunding, M. F., Rose, W. I., et al. (2017). Reference data set of volcanic ash physicochemical and optical properties. *Journal of Geophysical Research: Atmosphere*, *122*(17), 9485–9514. https://doi.org/10.1002/2016JD026328

Wagner, R., Kiselev, A., Möhler, O., Saathoff, H., & Steinke, I. (2016). Pre-activation of ice-nucleating particles by the pore condensation and freezing mechanism. *Atmospheric Chemistry and Physics*, *16*(4), 2025–2042. https://doi.org/10.5194/acp-16-2025-2016

Weidler, P. G., Luster, J., Schneider, J., Sticher, H., & Gehring, A. U. (1998). The Rietveld method applied to the quantitative mineralogical and chemical analysis of a ferralitic soil. *European Journal of Soil Science*, *49*(1), 95–105. https://doi.org/10.1046/j.1365-2389.1998.00138.x

Welti, A., Stetzer, O., Lohmann, U., & Lohmann, U. (2009). Atmospheric chemistry and physics influence of particle size on the ice nucleating ability of mineral dusts. *Atmospheric Chemistry and Physics*, *9*, 6705–6715. https://doi.org/10.5194/acp-9-6705-2009

Wilson, T. M., Stewart, C., Sword-Daniels, V., Leonard, G. S., Johnston, D. M., Cole, J. W., et al. (2012). Volcanic ash impacts on critical infrastructure. *Physics and Chemistry of the Earth*, *45–46*, 5–23. https://doi.org/10.1016/j.pce.2011.06.006

Wold, S., Esbensen, K., & Geladi, P. (1987). Principal component analysis. *Chemometrics and Intelligent Laboratory Systems*, *2*(1–3), 37–52. https://doi.org/10.1016/0169-7439(87)80084-9

Yano, E., Yokoyama, Y., Higashi, H., Nishii, S., Maeda, K., & Koizumi, A. (2010). Health effects of volcanic ash: A repeat study. *Archives of Environmental Health*, *45*(6), 367–373. https://doi.org/10.1080/00039896.1990.10118757

Young, K. C. (1993). *Microphysical processes in clouds*. Oxford University Press.

References From the Supporting Information

Fleet, R. E., Holdsworth, A. C., Morton, M. S., & Stoker, A. J. (1999). Geological society special publications series editor, santorini volcano. Geological Society.

Naranio, J. A., & Stern, C. R. (1998). Holocene explosive activity of Hudson Volcano, southern Andes. *Bulletin of Volcanology*, *59*(4), 291–306. https://doi.org/10.1007/s004450050193

Nye, C. J., & Turner, D. L. (1990). Petrology, geochemistry, and age of the Spurr volcanic complex, eastern Aleutian arc. *Bulletin of Volcanology*, *52*(3), 205–226. https://doi.org/10.1007/BF00334805

Rose, W. I., Penfield, G. T., Drexler, J. W., & Larson, P. B. (1980). Geochemistry of the andesite flank lavas of three composite cones within the Atitlán Cauldron, Guatemala. *Bulletin of Volcanology*, *43*(1), 131–153. https://doi.org/10.1007/BF02597617